OCS Study
BOEM 2015-049

Arctic Air Quality Modeling Study
Meteorological Model Performance Evaluation: 2009-2013 BOEM Arctic WRF Dataset

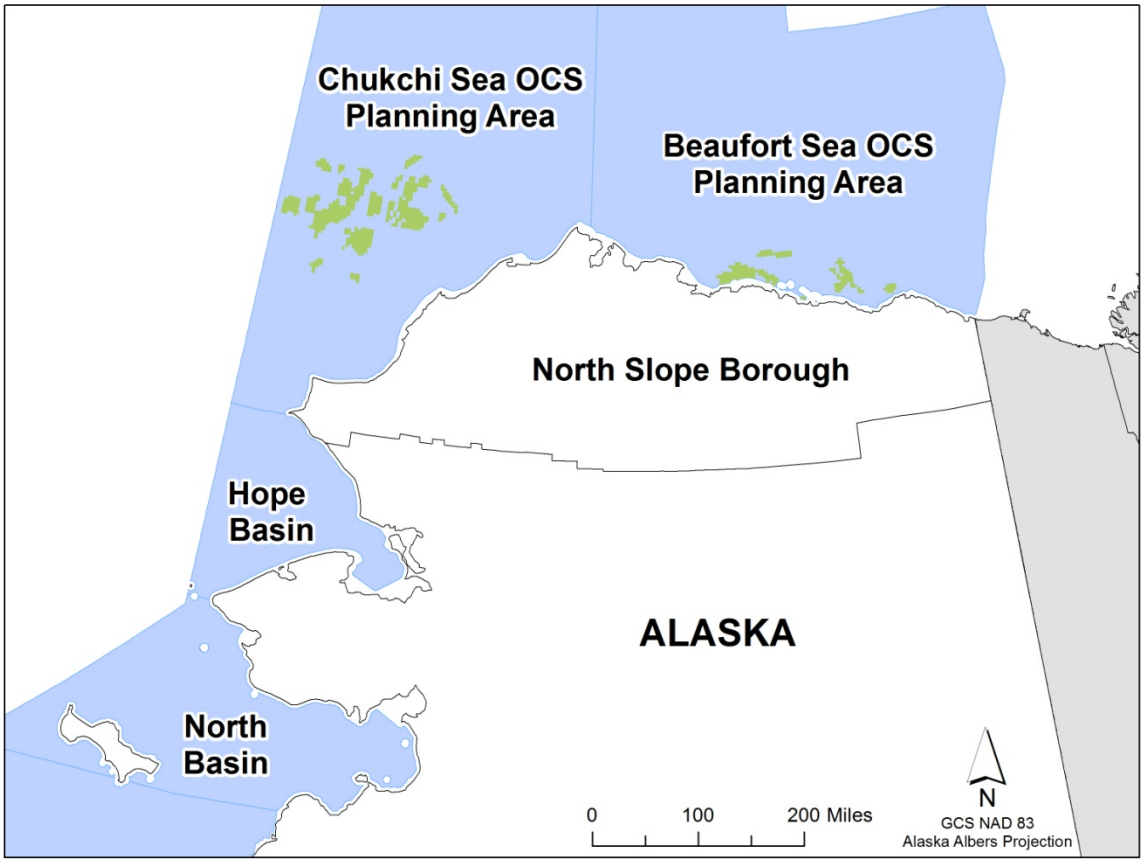

US Department of the Interior
Bureau of Ocean Energy Management
Alaska OCS Region

Eastern Research Group, Inc.
8950 Cal Center Drive
Suite 325
Sacramento, CA 95826

Ramboll Environ US Corporation
19020 33rd Ave. W.
Suite 310
Lynnwood, WA 98036-4754

[Page Intentionally Left Blank]

OCS Study
BOEM 2015-049

Arctic Air Quality Modeling Study
Meteorological Model Performance Evaluation: 2009-2013 BOEM Arctic WRF Dataset

Prepared by

Ramboll Environ US Corporation
19020 33rd Ave. W., Suite 310
Lynnwood, WA 98036-4754

Prepared for

U.S Department of Interior
Bureau of Ocean Energy Management
3801 Centerpoint Drive, Suite 500
Anchorage, AK 99503-5823

US Department of the Interior
Bureau of Ocean Energy Management
Alaska OCS Region

Eastern Research Group, Inc.
8950 Cal Center Drive
Suite 325
Sacramento, CA 95826

Ramboll Environ US Corporation
19020 33rd Ave. W.
Suite 310
Lynnwood, WA 98036-4754

January 18, 2016

Disclaimer

This report has been reviewed by the BOEM and approved for publication. Approval does not signify that the contents necessarily reflect the views and policies of the Bureau, nor does mention of trade names or commercial products constitute endorsement or recommendation for use.

May be cited as:
Brashers, B.; Knapik, J.; McAlpine, J.D.; Sturtz, T.; Morris, R. 2016. Arctic Air Quality Modeling Study – Meteorological Model Performance Evaluation: 2009-2013 BOEM Arctic WRF Dataset. Prepared by Ramboll Environ U.S. Corporation for U.S. Department of the Interior, Bureau of Ocean Energy Management. OCS Study BOEM 2015-049, 50 pp.

Authors:

Bart Brashers
Joe Knapik
JD McAlpine
Timothy Sturtz
Ralph Morris

METEOROLOGICAL MODEL PERFORMANCE EVALUATION

2009-2013 BOEM Arctic WRF Dataset

Table of Contents

Section **Page**

List of Figures

List of Tables

Abbreviations and Acronyms

AMSR	Advanced Microwave Scanning Radiometer
AQ	Air Quality
ARW	Advanced Research WRF
BOEM	Bureau of Ocean Energy Management
CCF	Cloud Cover Fraction
C-MAN	Coastal-Marine Automated Network stations
CMC	Canadian Meteorological Centre
ECMWF	European Center for Medium-range Weather Forecasting
ERG	Eastern Research Group, Inc.
EPA	US Environmental Protection Agency
FDDA	Four Dimensional Data Assimilation
JAMSTEC	Japan Agency for Marine-Earth Science and Technology
LCC	Lambert Conformal Conic map projection
LSM	Land-Surface Model
MADIS	Meteorological Assimilation Data Ingest System observation archive
METSTAT	Meteorological /Statistical Program
MISR	Multi-angle Imaging SpectroRadiometer
MMM	Meso-scale Meteorological Modeling
MPE	Model Performance Evaluation
NASA	National Aeronautics and Space Administration
NCAR	National Center for Atmospheric Research
NCEP	National Center for Environmental Prediction
NCDC	National Climatic Data Center
NDBC	National Data Buoy Center
NMM	Nonhydrostatic Mesoscale Model
NOAA	National Oceanographic and Atmospheric Administration
NODC	National Oceanographic Data Center
NWS	National Weather Service
PABR	Meteorological call sign for Point Barrow
PBL	planetary boundary layer
PRISM	Parameter-elevation Regressions on Independent Slopes Model
RMSE	Root Mean Square Error
RRTMG	Rapid Radiative Transfer Model for Global Climate Models
SCAS-OSU	Spatial Climate Analysis Service at Oregon State University
SIP	State Implementation Plan
SST	Sea Surface Temperature
UAF	University of Alaska Fairbanks
UTC	Universal Time Coordinate
WPS	WRF Pre-processing System
WRAP	Western Regional Air Partnership
WRF	Weather Research and Forecasting model
YSU	Yonsei University

1.0 INTRODUCTION

This report presents a model performance evaluation (MPE) of a Weather Research and Forecasting (WRF) model run, simulating the atmosphere of the North Slope of Alaska. The results being evaluated represent five years (2009-2013) of WRF meteorological modeling performed by Ramboll Environ. The purpose of the modeling is to provide the meteorological dataset to the Bureau of Ocean Energy Management (BOEM) for air quality (AQ) modeling in the Arctic. The Arctic AQ Modeling Study is being conducted under BOEM Contract Number M13PC00014 by the team of Eastern Research Group, Inc. (ERG) and Ramboll Environ US Corporation (Ramboll Environ) with assistance from the University of Alaska Fairbanks (UAF).

The BOEM Arctic WRF meteorological dataset was based on a previous EPA/BOEM WRF dataset with updates to improve performance in Northern Alaska. This assessment evaluates the BOEM Arctic WRF dataset on the bases of METSTAT, vertical profile, precipitation, and cloud cover outputs. The use of the METSTAT program and surface meteorological observations was used to evaluate WRF for wind speed, wind direction, temperature and mixing ratio. An evaluation of the vertical profile of WRF temperature and dew point temperature against twice daily upper-air observations from Point Barrow, Alaska was also completed. The PRISM model output was used to evaluate the spatial distribution and magnitudes of the WRF precipitation estimates. Finally, WRF cloud cover estimates were compared to satellite datasets in a qualitative manner.

2.0 METEOROLOGICAL MODELING

Over the past decade, emergent requirements for numerical simulation of urban and regional scale air quality have led to intensified efforts to construct high-resolution emissions, meteorological and air quality data sets. It is now possible, for example, to exercise sophisticated mesoscale prognostic meteorological models and Eulerian and Lagrangian photochemical/aerosol models for multi-seasonal periods over near-continental scale domains in a matter of weeks with the application tailored to a specific air quality modeling project.

The WRF model is the current preferred model for atmospheric research and operational forecasting needs at mesoscale resolution (approximately 5 to several hundred km). The model is the state-of-the-art atmospheric simulation system, commonly used to drive air quality dispersion models on the regional level.

The operational version of the model is the Nonhydrostatic Mesoscale Model (NMM) WRF core version 3, developed and maintained by the National Oceanic and Atmospheric Administration (NOAA) and the National Centers for Environmental Prediction (NCEP) (NOAA, 2015). The Advanced Research WRF (ARW) core, currently version WRF 3.7.1, is supported by the NCAR Mesoscale and Microscale Meteorology Division (NCAR, 2015). Based on extensive experience with mesoscale modeling in the Polar Regions by the Polar Meteorology Group of the Byrd Polar and Climate Research Center at The Ohio State University, WRF-ARW has been modified for use in the Polar Regions (referred to as the Polar WRF or PWRF). The modeling described in this report used PWRF version 3.6.1.

The WRF model contains separate modules to compute different physical processes such as surface energy budgets and soil interactions, turbulence, cloud microphysics, and atmospheric radiation. Within WRF, the user has many options for selecting the different schemes for each type of physical process. There is a WRF Pre-processing System (WPS) that generates the initial and boundary conditions used by WRF, based on topographic datasets, land use information, and larger-scale atmospheric and oceanic models.

2.1 Arctic Air Quality Meteorological Modeling

An evaluation by Ramboll Environ (Brashers et al., 2015) found the existing Arctic meteorological datasets to be insufficient for the needs of the Arctic Air Quality Modeling Study and recommended upgrading the configuration of the previous EPA/BOEM WRF to create a high-resolution, five-year dataset. An optimized version of the EPA/BOEM WRF dataset, known as the "BOEM Arctic WRF", was deemed necessary for use in air quality modeling within the Arctic Air Quality Modeling Study domain. This final BOEM Arctic WRF model configuration, evaluated in this report, is very similar to the initial EPA/BOEM WRF configuration, but differs from it in the following ways:

- Use of Polar WRF version 3.6.1 instead of version 3.4.1 used in the initial EPA/BOEM WRF.
- The inner-most 4 km domain was expanded slightly eastward, as shown in Figure 1.
- Use of the UKMO high resolution sea surface temperature (SST) dataset in place of the Real Time Global (RTG) dataset.
- Use of the Thompson microphysics scheme over the Morrison scheme.
- Use of the Grell-Freitas cumulus parameterization in the 36 km, 12 km, and 4 km domains instead of Kain-Fritsch scheme in the 36 km and 12 km domains.
- Increasing the time between radiation physics calls from 5 min to 20 min in all three domains.

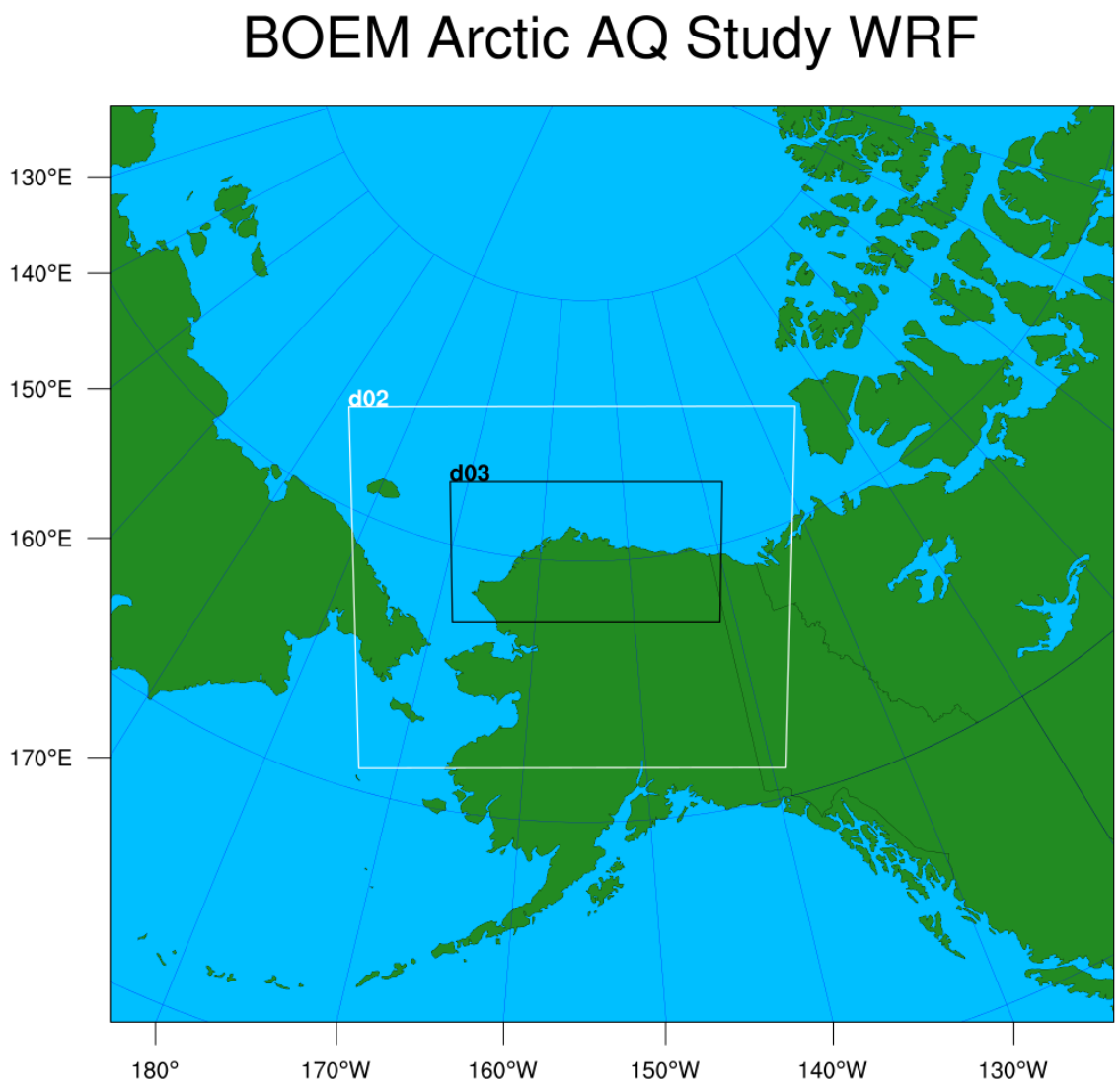

Figure 1. BOEM Arctic WRF Domains, 36km (full plot), 12km (d02) and 4km (d03) grid resolution

3.0 WRF MODELING METHODOLOGY

This chapter describes the methodology used for conducting the WRF simulation for the January 2009 through December 2013 modeling period and also describes the model configuration used in the final WRF application for the Arctic Air Quality Modeling Study.

3.1 Model Inputs and Configuration

A brief summary of the WRF configuration and input data used for this model performance evaluation is provided below.

3.1.1 *WRF Version and Options*

Model Selection: The Polar version of WRF version 3.6.1 was used for the BOEM Arctic simulation over the North Slope of Alaska. This version of the model was developed to improve WRF Arctic modeling capabilities (Hines and Bromwich 2008) (Bromwich, et al., 2009). Their modifications have focused on optimizing the surface energy budget and parameterization of sea-ice and permanent ice surfaces within the Noah land surface model (Chen, Janjic and Mitchell 1997). The modifications have included implementation of a variable sea-ice and snow thickness and seasonally-variable sea-ice albedo. The WPS pre-processor programs including GEOGRID, UNGRIB and METGRID were used to develop model inputs.

Topographic Inputs: Topographic information for the WRF was developed using the standard WRF terrain databases. The 36 km domain was based on the 10 minute (18 km) global data. The 12 km domain was based on the 2 minute (~4 km) data. The 4 km domain was based on the 30 second (~900 m) data.

Vegetation Type and Land Use Inputs: Vegetation type and land use information were developed using the most recently released WRF databases provided with the WRF distribution. Standard WRF surface characteristics corresponding to each land use category were employed.

Atmospheric Data Inputs: WRF relies on other model or re-analysis output to provide initial and boundary conditions (IC/BC). Typically, these are available in coarser time- and space-scales than WRF produces, e.g. approximately 70 km and 6-hourly for the European Centre for Medium-Range Weather Forecasts (ECMWF) interim reanalysis dataset (ERA-Interim). These were objectively re-analyzed using traditional observational data (meteorological towers) to the higher resolution of each WRF grid, using the OBSGRID program. These fields are used both to initialize the model, and to perform analysis nudging to guide the model to best match the observations.

Time Integration: Third-order Runge-Kutta integration was used with a variable time step of 120 to 90 seconds for the 36 km domain, 60 to 30 seconds for the 12 km domain, and 20 to 10 seconds for the 4 km domain.

Diffusion Options: Horizontal Smagorinsky first-order closure with sixth-order numerical diffusion and suppressed up-gradient diffusion was used.

Lateral Boundary Conditions: Lateral boundary conditions were specified from the initialization dataset on the 36 km domain with continuous updates nested from the 36 km domain to the 12 km Alaskan domain and continuous updates nested from the 12 km domain to the 4 km North Slope domain.

Top and Bottom Boundary Conditions: The top boundary condition was selected as an implicit Rayleigh dampening for the vertical velocity. Consistent with the model application for non-idealized cases, the bottom boundary condition was selected as physical, not free-slip.

Water Temperature Inputs: The UK Met Office's (UKMO) Operational Sea Surface Temperature and Sea Ice Analysis dataset was selected after extensive testing of several SST databases. The UKMO's SST analysis uses a spatial resolution of 0.054 degree (~6 km

resolution). The UKMO SST dataset was chosen for the lowest bias and error in model performance evaluation tests during open water periods and its graphical similarity depicting the Beaufort Sea and Mackenzie River discharge in summer.

Snow Depth/Sea Ice Thickness Inputs: The runs used the 24 km resolution snow/ice data from the Canadian Meteorological Centre (CMC) Daily Snow Depth Analysis to supply the input snow cover over land. Additionally, the BOEM Arctic WRF runs used three over-ocean datasets developed by the Ohio State University Polar Meteorology Group. Dr. Hines, of the Ohio State University Polar Meteorology Group, supplied datasets of sea ice thickness, snow-on-ice thickness, and sea ice/snow albedo based on radiances collected by the Advanced Microwave Scanning Radiometer (AMSR). These data were used as input fields for Polar WRF. Although WRF writes these fields in its output, they are not predicted fields, only "passed through" from the inputs.

FDDA Data Assimilation: The WRF model was run with a combination of analysis and observation nudging (i.e., Four Dimensional Data assimilation [FDDA]). Analysis nudging was used for winds, temperature, and humidity on the 36 and 12 km domains above the planetary boundary layer (PBL) height in both the initial and final WRF simulations. The WRF simulation used observation nudging within the 4 km domain for winds, temperature, and humidity. The nudging used both surface and aloft nudging, but nudging for temperature and mixing ratio was not performed in the lower atmosphere (i.e., within the boundary layer). Observation nudging for winds and temperature was performed on the 4 km grid domain using the Meteorological Assimilation Data Ingest System (MADIS)[1] observation archive. The MADIS archive includes the National Climatic Data Center (NCDC)[2] observations and the National Data Buoy Center (NDBC) Coastal-Marine Automated Network C-MAN[3] stations.

Physics Options: The WRF model contains many different physics options. The physics options chosen for the BOEM Arctic WRF configuration are summarized in Table 1. See the WRF User's Guide[4] or its Physics References page[5] for more details on each option.

Application Methodology: The WRF model was executed in 5-day blocks initialized at 12Z every 5 days. Model results were output every 60 minutes and output files were split at 12 hour intervals. Twelve (12) hours of spin-up were included in each 5-day block before the data were used in the subsequent evaluation. The model was run at the 36, 12 and 4 km resolution from January 2009 through December 2013.

[1] Meteorological Assimilation Data Ingest System. http://madis.noaa.gov/
[2] National Climatic Data Center. http://lwf.ncdc.noaa.gov/oa/ncdc.html
[3] National Data Buoy Center. http://www.ndbc.noaa.gov/cman.php
[4] WRF User's Guide. http://www2.mmm.ucar.edu/wrf/users/docs/user_guide_V3/contents.html
[5] WRF Physics References http://www2.mmm.ucar.edu/wrf/users/wrfv3.5/phys_references.html

Table 1. Physics Options used in the BOEM Arctic WRF Dataset

Physics	Parameterization Scheme	Description
Long/Shortwave Radiation	Rapid Radiative Transfer Model for GCM (RRTMG)[6]	Scheme with the MCICA method of random cloud overlap
Micro-physics	Thompson[6]	Scheme with ice, snow and graupel processes suitable for high-resolution simulations
Cumulus physics	Grell-Freitas[6]	Scheme that tries to smooth the transition to cloud-resolving scales
Planetary boundary layer (PBL)	Yonsei University (YSU)[6]	Scheme with explicit entrainment layer and parabolic K profile in unstable mixed layer
Land surface model (LSM)	NOAH[6] with Polar WRF modifications	Scheme with soil temperature and moisture in four layers, fractional snow cover and frozen soil physics

3.1.2 *Domain Configuration*

The WRF domain configuration is comprised of a system of simultaneous nested grids. All WRF grids are defined on a Lambert Conformal Conic (LCC) projection centered at 70°N, 155°W with true latitudes at 70°N. The final dataset was produced using three domains as show in Figure 1: a 4 km resolution domain centered on the Northern Alaska coast, a 12 km domain that encompasses most of Alaska and the Beaufort and Chukchi Seas and an extended 36 km domain designed to capture synoptic scale features (full plot). Table 2 provides the input configurations for the WRF domains used in this project. NX and NY are the number of east-west and north-south staggered grid points, respectively, in each domain. I-start and J-start indicate the western and southern nested grid starting indices with respect to the parent grid. Geographic Resolution relates to the geographic datasets employed for each grid, in terms of minutes or seconds of degrees.

Table 2. BOEM Arctic WRF Domain Configuration

Grid Resolution	NX	NY	I-start	J-start	Geographic Resolution	Coverage
36 km	120	110	1	1	10 minute	NW North America & NE Russia
12 km	157	130	33	31	2 minute	Alaska
4 km	289	151	36	53	30 second	N Alaska

[6] WRF ARW Version 3 Modeling System User's Guide http://www2.mmm.ucar.edu/wrf/users/docs/user_guide_V3/users_guide_chap5.htm#

3.1.3 *Model Vertical Resolution*

High vertical resolution enables the model to more accurately capture low level inversions frequently present throughout the winter months. The WRF modeling was based on 34 vertical layers with levels packed near the surface in an attempt to improve the simulation atmospheric boundary layer structure and processes, shown in Table 3.

Table 3. BOEM Arctic WRF Dataset Model Levels

Level	eta	Pressure (mb)	Height (m)	Mid Height (m)	Thickness (m)
0	1	1000	0.0		
1	0.9985	999	11.6	5.8	11.6
2	0.997	997	23.2	17.4	11.6
3	0.995	996	38.7	30.9	15.5
4	0.992	993	62.0	50.3	23.3
5	0.987	988	100.9	81.4	38.9
6	0.98	982	155.6	128.2	54.7
7	0.97	973	234.3	194.9	78.7
8	0.96	964	313.5	273.9	79.3
9	0.95	955	393.4	353.4	79.9
10	0.94	946	473.8	433.6	80.5
11	0.93	937	554.9	514.4	81.1
12	0.915	924	677.8	616.3	122.8
13	0.90	910	802.1	739.9	124.3
14	0.88	892	970.1	886.1	168.1
15	0.85	865	1227.4	1098.8	257.3
16	0.82	838	1491.3	1359.4	263.9
17	0.78	802	1854.1	1672.7	362.8
18	0.74	766	2230.4	2042.3	376.2
19	0.70	730	2621.2	2425.8	390.8
20	0.64	676	3237.8	2929.5	616.6
21	0.58	622	3895.7	3566.8	657.9
22	0.52	568	4601.6	4248.6	705.9
23	0.455	510	5430.5	5016.0	828.9
24	0.40	460	6194.4	5812.5	763.9
25	0.35	415	6949.1	6571.7	754.6
26	0.30	370	7773.2	7361.1	824.1
27	0.25	325	8682.9	8228.0	909.7
28	0.20	280	9701.0	9191.9	1018.1
29	0.15	235	10861.6	10281.3	1160.6
30	0.10	190	12218.6	11540.1	1357.1
31	0.06	154	13506.9	12862.8	1288.3
32	0.027	124	14768.9	14137.9	1262.0
33	0	100	15998.6	15383.8	1229.7

4.0 WRF MODEL PERFORMANCE EVALUATION RESULTS

The model performance evaluation using the WRF configuration described herein includes a quantitative and qualitative component. The quantitative evaluation compares surface meteorological observations with corresponding WRF predictions at specific times and locations. The qualitative evaluation performs a larger-scale comparison of spatial fields of meteorological observations with gridded WRF fields.

4.1 Quantitative Evaluation Using METSTAT

4.1.1 *Quantitative Statistics*

A quantitative model performance evaluation of the BOEM Arctic WRF simulation was performed using surface meteorological measurements and the publicly-available METSTAT evaluation tool. METSTAT calculates statistical performance metrics for bias, error and correlation for surface winds, temperature, and mixing ratio (i.e., water vapor or humidity). To evaluate the performance of a meteorological model simulation for air quality model applications, a number of performance benchmarks for comparison are typically used. Table 4 lists the meteorological model performance benchmarks for simple (Emery et al., 2001) and complex (Kemball-Cook et al., 2005) situations. The simple benchmarks were developed by analyzing well-performing meteorological model evaluation results for simple, mostly flat terrain conditions and simple meteorological conditions (e.g., stationary high pressure) that were mostly conducted to support air quality modeling studies (e.g., ozone State Implementation Plan [SIP] modeling). The complex benchmarks were developed during the Western Regional Air Partnership (WRAP) regional haze modeling and are performance benchmarks for more complex conditions, such as the complex terrain of the Rocky Mountains and Alaska (Kemball-Cook et al., 2005). McNally (2009) analyzed multiple annual runs that included complex terrain conditions and suggested an alternative set of benchmarks for temperature and humidity under more complex conditions. The purpose of the benchmarks is to understand how good or poor the results are relative to other model applications run for the United States.

In this section, Ramboll Environ compared the WRF meteorological statistics to the benchmarks as an indication of the BOEM Arctic WRF model performance. These benchmarks include bias and error in temperature, wind direction and mixing ratio as well as the wind speed bias and Root Mean Squared Error (RMSE) between the model and observations.

Because air dispersion models are all statistically-based and use meteorology as a statistical sample of meteorological conditions, the timing of specific conditions matters less than that a condition occurred during the modeling period. The WRF model generally has some error in predicting the timing of the passage of surface cold/warm fronts. Errors in frontal passage timing can enhance errors in certain statistics, e.g. temperature and wind direction. These errors do not necessarily predict poor performance of air dispersion models that use the WRF data, as air dispersion models are typically evaluated on longer timescales or using “disaggregated in time” statistics.

Table 4. Meteorological Model Performance Benchmarks for Simple and Complex Conditions

Parameter	Emery et al. (2001)	Kemball-Cook et al. (2005)	McNally (2009)	Resulting Criteria
Conditions	Simple	Complex	Complex	Complex
Temperature Bias	≤ ±0.5 K	≤ ±2.0 K	≤ ±1.0 K	≤ ±1.0 K
Temperature Error	≤ 2.0 K	≤ 3.5 K	≤ 3.0 K	≤ 3.0 K
Temperature IOA	≥ 0.8	(not addressed)	(not addressed)	≥ 0.8
Humidity Bias	≤ ±1.0 g/kg	≤ ±0.8 g/kg	≤ ±1.0 g/kg	≤ ±1.0 g/kg
Humidity Error	≤ 2.0 g/kg	≤ 2.0 g/kg	≤ 2.0 g/kg	≤ 2.0 g/kg
Humidity IOA	≥ 0.6	(not addressed)	(not addressed)	≥ 0.6
Wind Speed Bias	≤ ±0.5 m/s	≤ ±1.5 m/s	(not addressed)	≤ ±1.5 m/s
Wind Speed RMSE	≤ 2.0 m/s	≤ 2.5 m/s	(not addressed)	≤ 2.5 m/s
Wind Speed IOA	≥ 0.6	(not addressed)	(not addressed)	≥ 0.6
Wind Dir. Bias	≤ ±10 degrees	(not addressed)	(not addressed)	≤ ±10 degrees
Wind Dir. Error	≤ 30 degrees	≤ 55 degrees	(not addressed)	≤ 55 degrees

The output from the BOEM Arctic WRF simulation was compared against the global-scale NCDC DS-3505 observational data, and against data from the buoys stored in the NOAA National Oceanographic Data Center (NODC) database. Typical measurement errors for onshore stations can be found in FAA Advisory Circular No: 150/5220-16D[7], and for buoys at the NDBC's website.[8] For example, onshore wind speed sensors are accurate to within 1 knot (0.5 m/s) for ultrasonic anemometers and 2 knots (1.0 m/s) for cup anemometers, with wind direction accurate to with 3 to 5 degrees RMSE, respectively. Buoy wind measurements are less accurate, at ±1.0 m/s (speed) and ±10 degrees (direction).

A standard set of statistical metrics from the METSTAT package was used. These metrics were calculated on hourly, daily and monthly time frames for wind speed, wind direction, temperature, and humidity at the surface; using all available observational weather data.

The WRF surface meteorological model performance metrics were compared against the simple and complex model performance goals using "soccer plots." Soccer plots display two WRF performance metrics on the x-axis and y-axis (e.g., monthly-averaged temperature bias and error) along with the performance benchmarks. Generally, the closer the symbols are to the origin, the better the model performance. It is also easy to see when a WRF performance metric falls within the benchmark lines (i.e., score a goal). Below we present example monthly surface meteorological model performance across the 4 km North Slope Alaska domain (domain d03).

4.1.2 *Onshore METSTAT Evaluation*

METSTAT was used to evaluate onshore model performance of the BOEM-Arctic WRF dataset using the National Climate Data Center's (NCDC) global-scale quality-controlled DS-3505 integrated surface hourly observational data as verification data (NOAA-NCDC, 2014). Global

[7] FAA AWOS Advisory http://www.faa.gov/documentLibrary/media/Advisory_Circular/150-5220.16D.pdf
[8] NDBC accuracy tables http://www.ndbc.noaa.gov/rsa.shtml

hourly and synoptic observations are compiled from numerous sources into a single common ASCII format and common data model. The DS-3505 database contains records of most official surface meteorological stations from airports, military bases, reservoirs/dams, agricultural sites, and other sources dating from 1901 to the present. Quality control of the data has corrected well over 99% of the errors present in the original data (NOAA-NCDC, 2015).

The onshore METSTAT soccer plot results for BOEM Arctic WRF wind direction performance in the 4 km domain are shown in Figure 2. Wind direction performed very well with all months meeting the simple conditions benchmark. Figure 3 shows humidity performance in the 4 km domain. Again, WRF performed very well with each month falling within the simple conditions benchmark with biases ranging from -0.4 to 0.4 g/kg. Wind speed performance for the 4km domain is shown in Figure 4. WRF performed well with a small wind speed bias, but a RMSE ranging from 1.5 m/s to 2.5 m/s – approximately half of the months fall within the simple conditions benchmark and the other half within the complex conditions. The fall and winter months generally display a higher wind speed error throughout the year, compared to the open-water periods.

Figure 5 displays soccer plot results for temperature performance for the 4 km domain. BOEM Arctic WRF performed reasonably well with a majority of months falling within the complex conditions benchmark, but only several months within the simple conditions benchmark. Monthly plots display a negative temperature bias overall with increased temperature error 2.0 to 4.5 K for the winter months (particularly 2010) and decreased temperature error of 1.0 to 2.0 K for the open water months. The outliers are winter months from each year and display a very negative (cold) temperature bias, outside of the complex condition benchmark. The WRF model's under-prediction of temperatures is likely due to the persistent ice coverage throughout the late fall, winter and early spring months.

Overall, WRF performed well compared to onshore surface observations for wind speed, wind direction, humidity and temperature for all months in the five-year dataset. For 2012 in particular, only one or two month-parameter combinations fell outside the complex condition benchmarks.

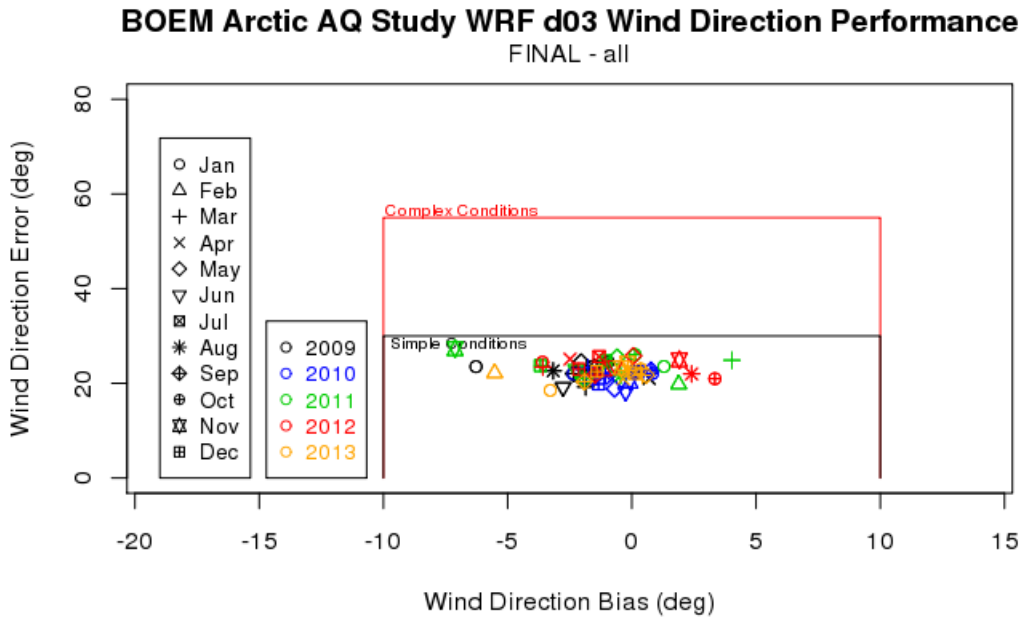

Figure 2. BOEM Arctic WRF Onshore METSTAT d03 Wind Direction Performance

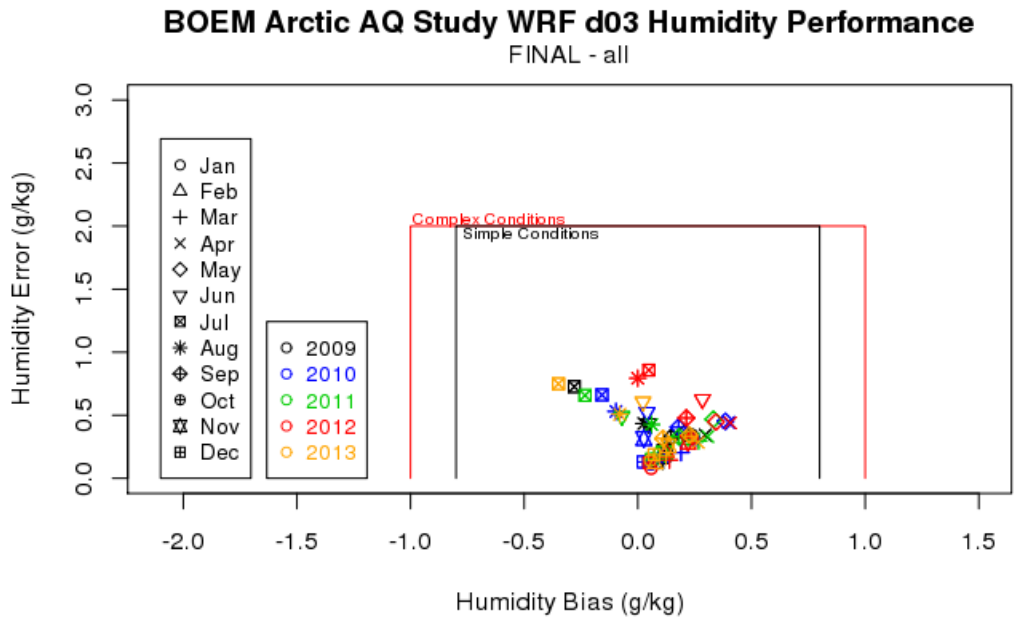

Figure 3. BOEM Arctic WRF Onshore METSTAT d03 Humidity Performance

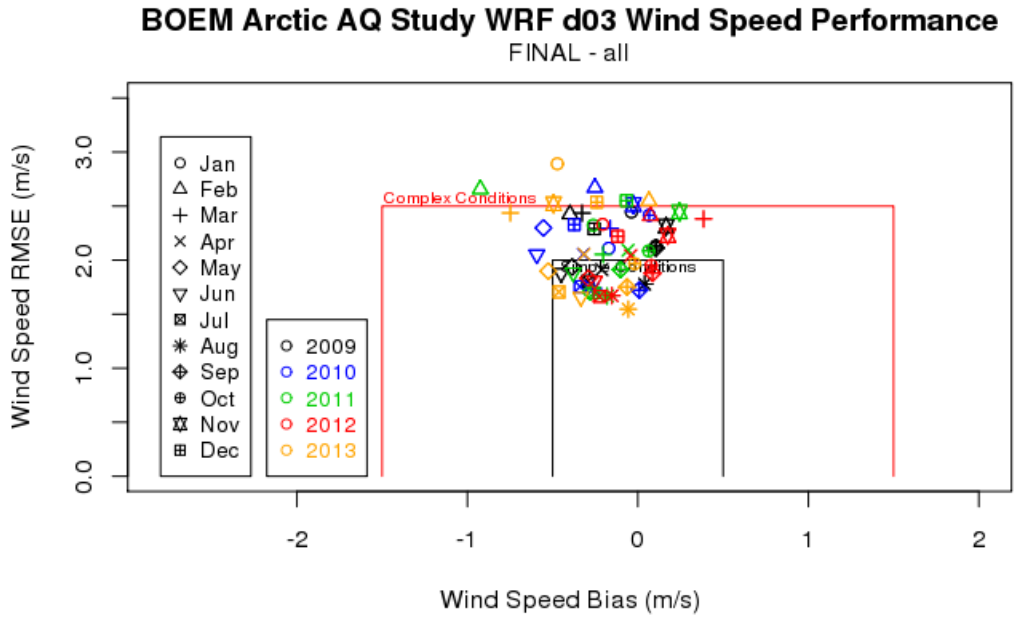

Figure 4. BOEM Arctic WRF Onshore METSTAT d03 Wind Speed Performance

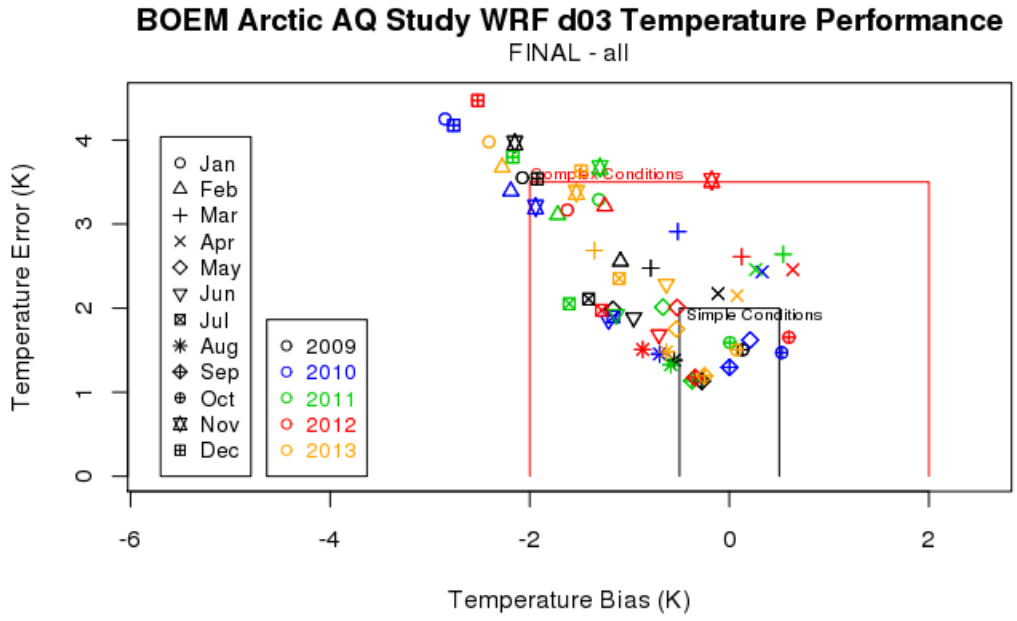

Figure 5. BOEM Arctic WRF Onshore METSTAT d03 Temperature Performance

4.1.3 *Offshore METSTAT Evaluation*

METSTAT was used to evaluate WRF performance using observations from meteorological buoys stored in the NOAA National Oceanographic Data Center (NODC) database. The observation datasets used for the METSTAT analysis included the data collected by shipboard and moored meteorological buoy data collected in the Chukchi Sea from NODC Accession 0093399 (NOAA-NODC, 2014). The originator of each Accession performs QA/QC on the data prior to uploading to the NODC database, and the accuracy of the observations may be lower, compared to that of a quality-controlled DS3505 database. Note that the buoys deployed in 2012 and 2013 only reported temperature, not winds or humidity.

Because the WRF output fields related to sea ice are simply "passed through" from the input dataset, no assessment of their performance was attempted. A discussion of the uncertainty of the satellite AMSR sensor and many of the derived products is available from the National Snow and Ice Data Center.[9]

The offshore METSTAT soccer plot results for BOEM Arctic wind direction performance in the 4 km domain are shown in Figure 6. A majority of months displayed a slight positive bias with an. The average direction error was in the 20-45 degree range, with all months falling within the complex conditions benchmark and about half the months falling within the simple conditions benchmark.

The WRF model performed very well for humidity, with all open water months within the simple conditions benchmark as shown in Figure 7. In Figure 8, there is overall a small positive wind speed bias for the periods of open water. October of 2009, 2010, and 2012 have wind speed errors of 2.5 to 3.5 m/s, falling outside the complex conditions threshold indicating that the model had difficulties in the transition month. Temperature performance is shown in Figure 9, with a majority of the open water months within the simple conditions benchmark. Most temperature plots display a slight negative bias, suggesting WRF is under-predicting temperatures during the warmer months.

Overall, WRF performance is satisfactory when compared to offshore observations. The offshore METSTAT performance appears less accurate compared to onshore METSTAT performance. This apparent difference is partly a result of the small number of available buoys relative to the number of stations onshore, because positive errors from one station and negative errors from another station can give average results that appear unbiased. The larger the number of stations in an average, the more likely they balance out. There is also a high frequency of missing observations in the NODC dataset.This speaks to the inherent difficulty in taking measurements in this geographic area, where the sea swell may be much larger than the height of the buoy mast, and the wind speed may be very high.

[9] AMSR uncertainties https://nsidc.org/data/amsre/data-quality/data-uncertainty.html

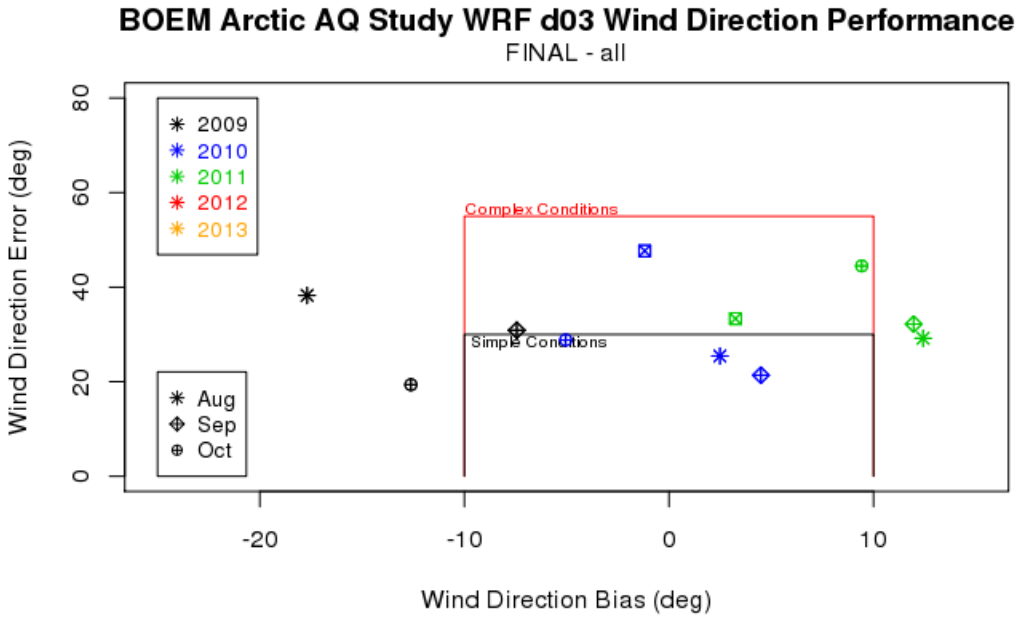

Figure 6. BOEM Arctic WRF Offshore METSTAT d03 Wind Direction Performance

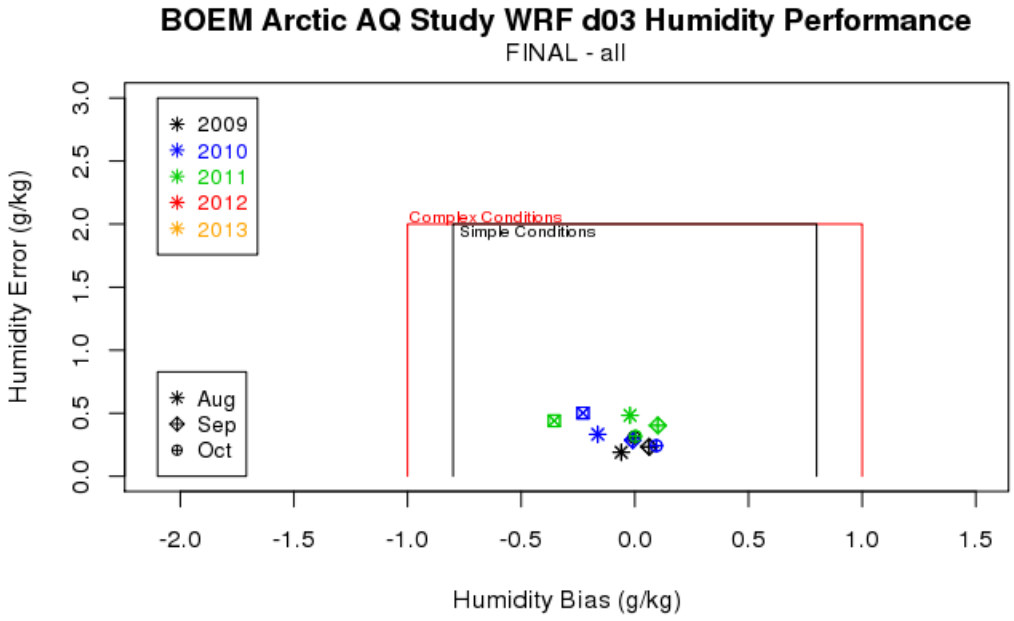

Figure 7. BOEM Arctic WRF Offshore METSTAT d03 Humidity Performance

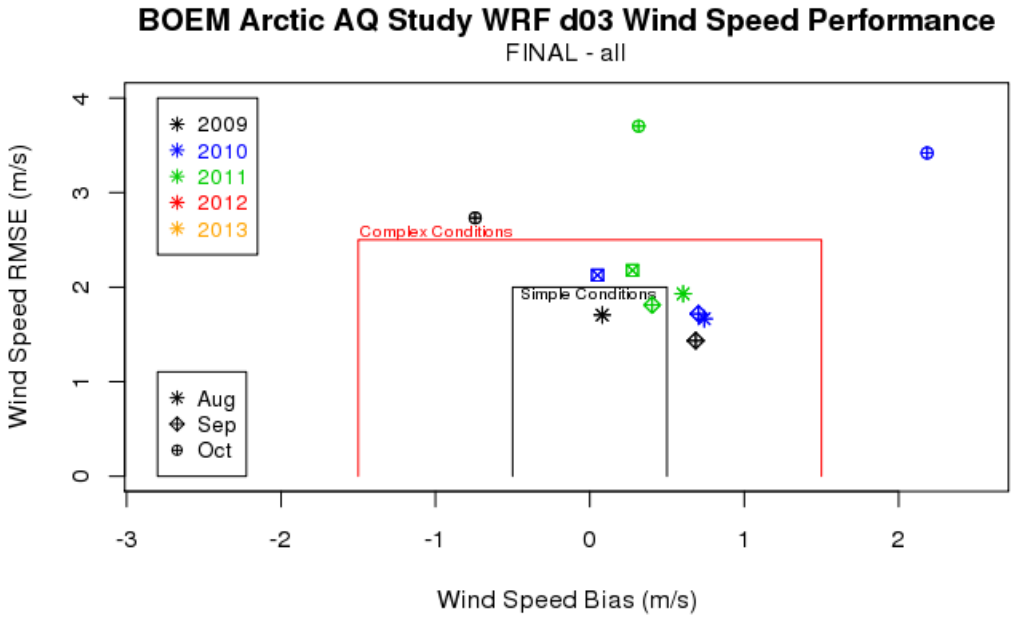

Figure 8. BOEM Arctic WRF Offshore METSTAT d03 Wind Speed Performance

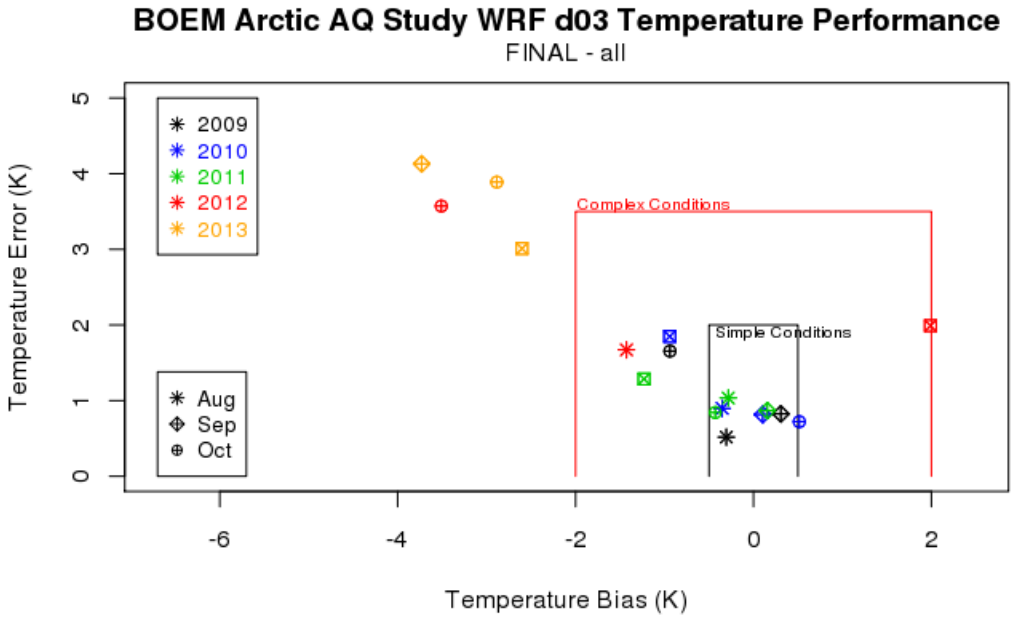

Figure 9. BOEM Arctic WRF Offshore METSTAT d03 Temperature Performance

4.2 Qualitative Evaluation Using Upper-Air Data

These analyses were conducted using upper air observation datasets within the study domain at Point Barrow, Alaska, which have time frames that overlap with the WRF modeling.

Upper-air data from the Point Barrow radiosonde (PABR) dataset were used to evaluate WRF vertical profiles of predicted temperature and moisture above that location. The PABR radiosonde dataset is collected by and maintained by the National Weather Service (NWS). Radiosondes are launched from PABR twice per day, at approximately 0 and 12 UTC. Radiosondes provide high-resolution vertical profiles of temperature, humidity, wind speed, and wind direction throughout the troposphere. The data are made publically available by NOAA on the Earth System Research Laboratory (ESRL) Radiosonde Observation website (www.esrl.noaa.gov/raobs). Ramboll Environ downloaded and stored the radiosonde data from 2009 to 2013 in FSL output format for use in WRF model dataset comparisons. The advantage of traditional radiosonde datasets are the length of the dataset (long periods at the same location) and the fact that they are direct measurements (as opposed to remote sensing). Disadvantages include the low frequency at only twice per day, and the fact that the lowest reported level comes from a different sensor than the rest of the profile and may occasionally lead to un-physical profiles. The measurement from the stationary sensor may be warmer than the lowest layer reported by the radiosonde, an unstable situation where the air would normally mix rapidly and the temperature gradient would be erased. Layers of temperature data showing super-adiabatic lapse rates are categorized as valid if the decrease in potential temperature in the layer does not exceed 1.0 K (NOAA-OFCM, 1997).

4.2.1 *Point Barrow Soundings*

Figures 10 through 14 show a selection of upper air profile plots taken from each year of the dataset for a sampling of several different atmospheric situations and WRF performance. The selection was made to show some of the worst-performing days, some of the best-performing days, and some in between. Figure 10 depicts vertical sounding profiles from the BOEM Arctic WRF dataset from April 21, 2009 on the left panel and July 6, 2009 on the right panel at Point Barrow. An elevated temperature inversion originates from around 350 meters above the surface and extends vertically to around 500 meters on the left panel. WRF overestimates the base and depth of the inversion. On the right panel, WRF estimates the depth of the surface inversion well, which extends to around 300 meters above the surface, but under-forecasts the surface temperature by a degree Celsius.

WRF predicts the temperature and moisture well for September 5, 2010 in Figure 11. WRF follows the elevated temperature inversion from 200 meters above the surface to around 400 meters. In the left panel for May 1, 2010, the model overestimates the surface temperature and underestimates the moisture in the upper levels, but follows the temperature closely through the lower-levels of the profile.

On the left panel in Figure 12, WRF represents the strong subsidence inversion well for June 8, 2011. On the right panel, for October 2, WRF under-predicts the surface temperature by three degrees Celsius, but represents the temperature and moisture well through the rest of the vertical profile.

Figure 13 displays the sounding from September 24, 2012 on the left panel and from November 12, 2012 on the right panel. The WRF model depicts the temperature inversion beginning too shallow on the left panel, but forecasts the height of the inversion accurately to around 500 meters from the surface. On the right panel, WRF under-forecasts the height of the subsidence inversion by 500 meters.

On the left panel in Figure 14, WRF underestimates the surface temperature by 7 degrees Celsius for January 4, 2013 but does represent the very strong inversion that begins at 200 meters above the surface and continues to warm nearly 17 degrees Celsius in 200 meters. On the right panel for July 7 2013, WRF represents both temperature and moisture well throughout the vertical column. Overall, WRF performs well representing temperature and moisture in the vertical profiles of the atmosphere below 2,000 feet, including surface and subsidence-type inversions.

4.2.2 *Other Upper-Air Datasets*

Brashers et al. (2015), used two other sources of upper-air data to assess WRF performance, namely the Japan Agency for Marine-Earth Science and Technology (JAMSTEC) cruise radiosonde data, and the Endeavor Island microwave thermal profiler data.

The JAMSTEC cruises are carried out by a Japanese research group to study various subjects relating to the world's oceans and climate. The cruises have been ongoing since 1987. The Research Vessel Mirai is a Japanese oceanographic research vessel that has been used for a series of JAMSTEC cruises to the Arctic Ocean as part of the JAMSTEC Arctic Ocean Climate System Research Project. Many separate legs from 1999 to 2013 were conducted that took the Mirai into the Arctic waters. Radiosonde measurements were collected on several of these legs, several of which overlap the WRF dataset periods.

The Endeavor Island upper-air profiler dataset consists of hourly records of temperature in the lower layers of the atmosphere collected from May 15, 2010 to February 28, 2013. Endeavor Island is a small man-made island located at the Endicott development approximately 15 miles east of Prudhoe Bay. A set of meteorological equipment is maintained on the island, including a traditional meteorological tower (measuring wind speed and direction, temperature, and humidity) and a Kipp & Zonen microwave thermal profiler.

Brashers et al. (2015) assessed a different, yet related, WRF dataset. The SST inputs used in that WRF run were found to have problems related to the Mackenzie River outflow, which caused poor WRF performance in the eastern part of the domain. That discovery led to a new WRF run, the subject of this report.

Because the locations of the JAMSTEC cruises and Endeavor Island are far from the areas that suffered from poor characterization of the SST, the WRF performance compared to the JAMSTEC and profiler datasets is expected to be similar for both the WRF run covered in Brashers et al. (2015) and the WRF run covered in this report. The reader is referred to Brashers et al. (2015), Section 4.3.

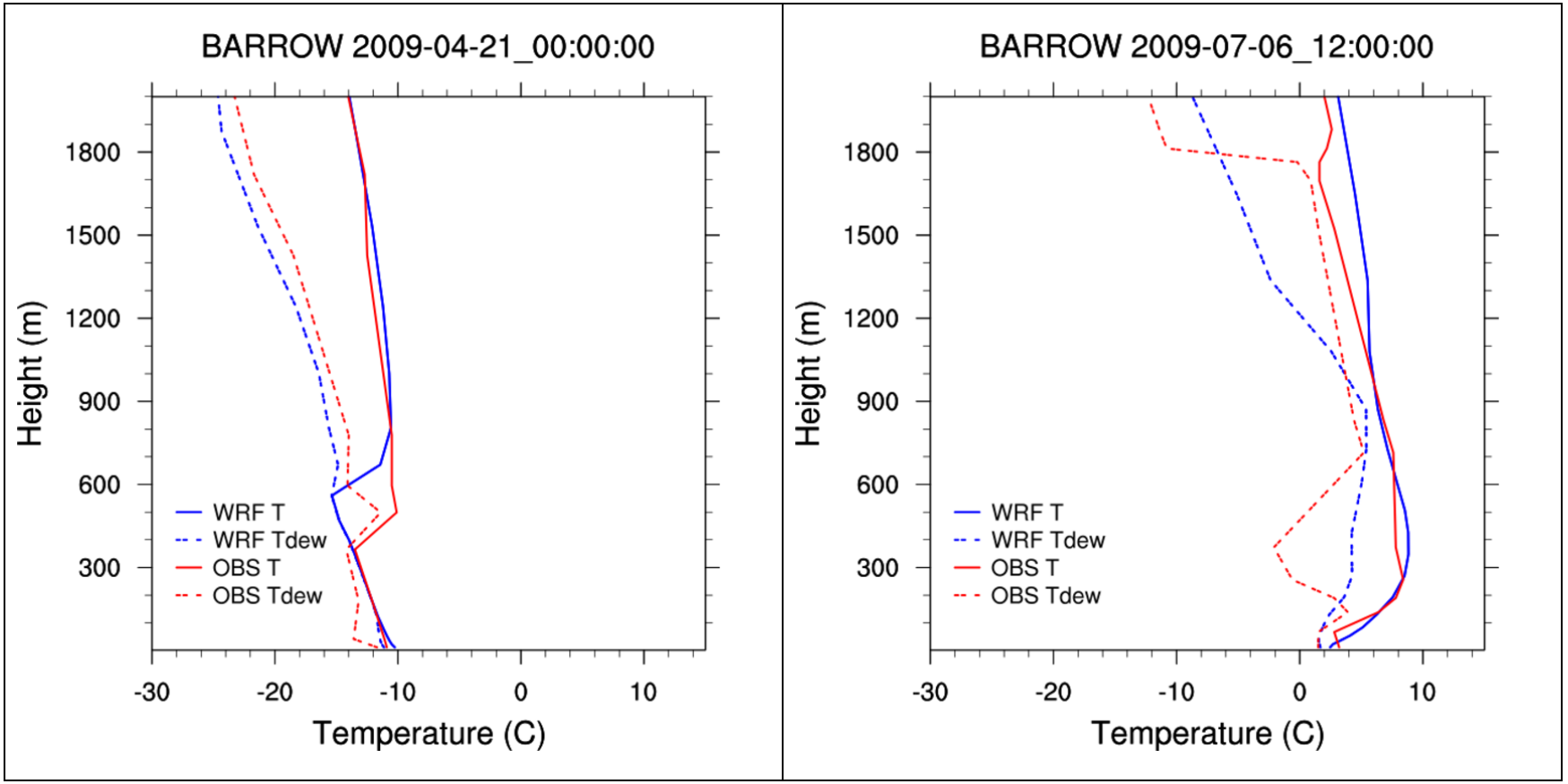

Figure 10. Vertical profile soundings comparing BOEM Arctic WRF to upper-air data at Point Barrow, AK (PABR) on April 21, 2009 at 00 UTC and July 6, 2009 at 12 UTC

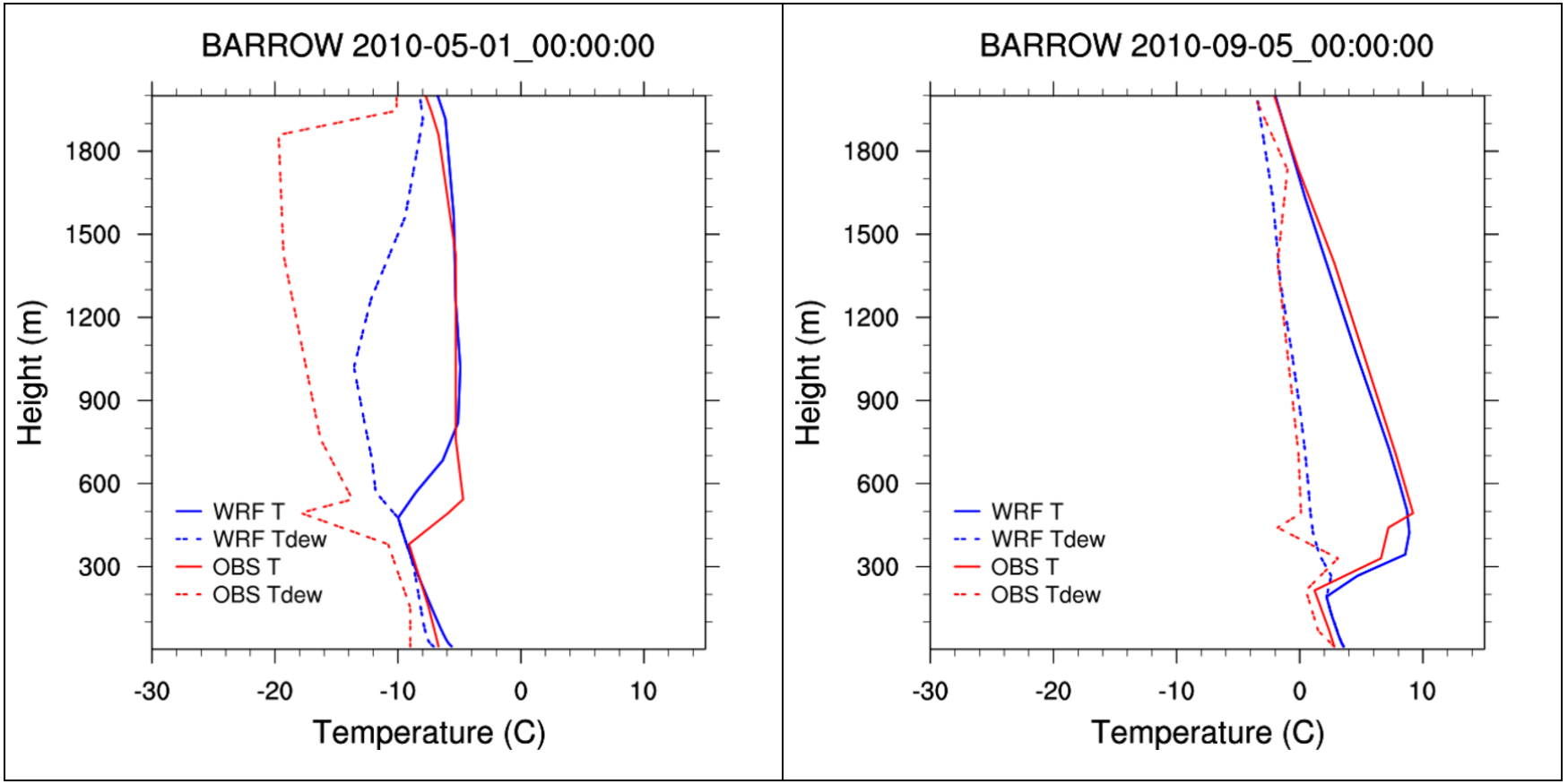

Figure 11. Vertical profile soundings comparing BOEM Arctic WRF to upper-air data at Point Barrow, AK (PABR) on May 1, 2010 at 00 UTC, and September 5, 2010 at 00 UTC

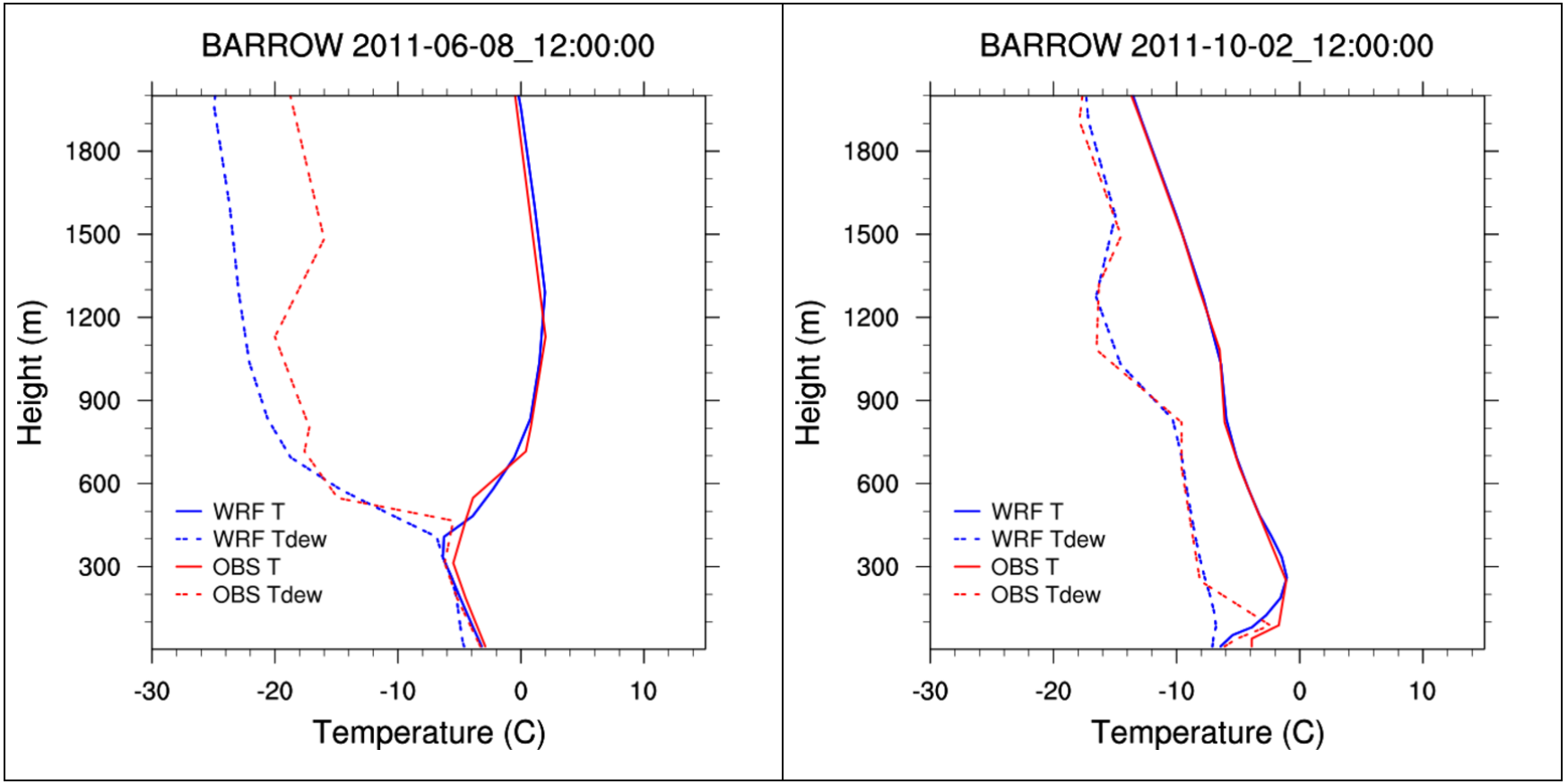

Figure 12. Vertical profile soundings comparing BOEM Arctic WRF to upper-air data at Point Barrow, AK (PABR) on June 8, 2011 at 12 UTC and October 2, 2011 at 12 UTC

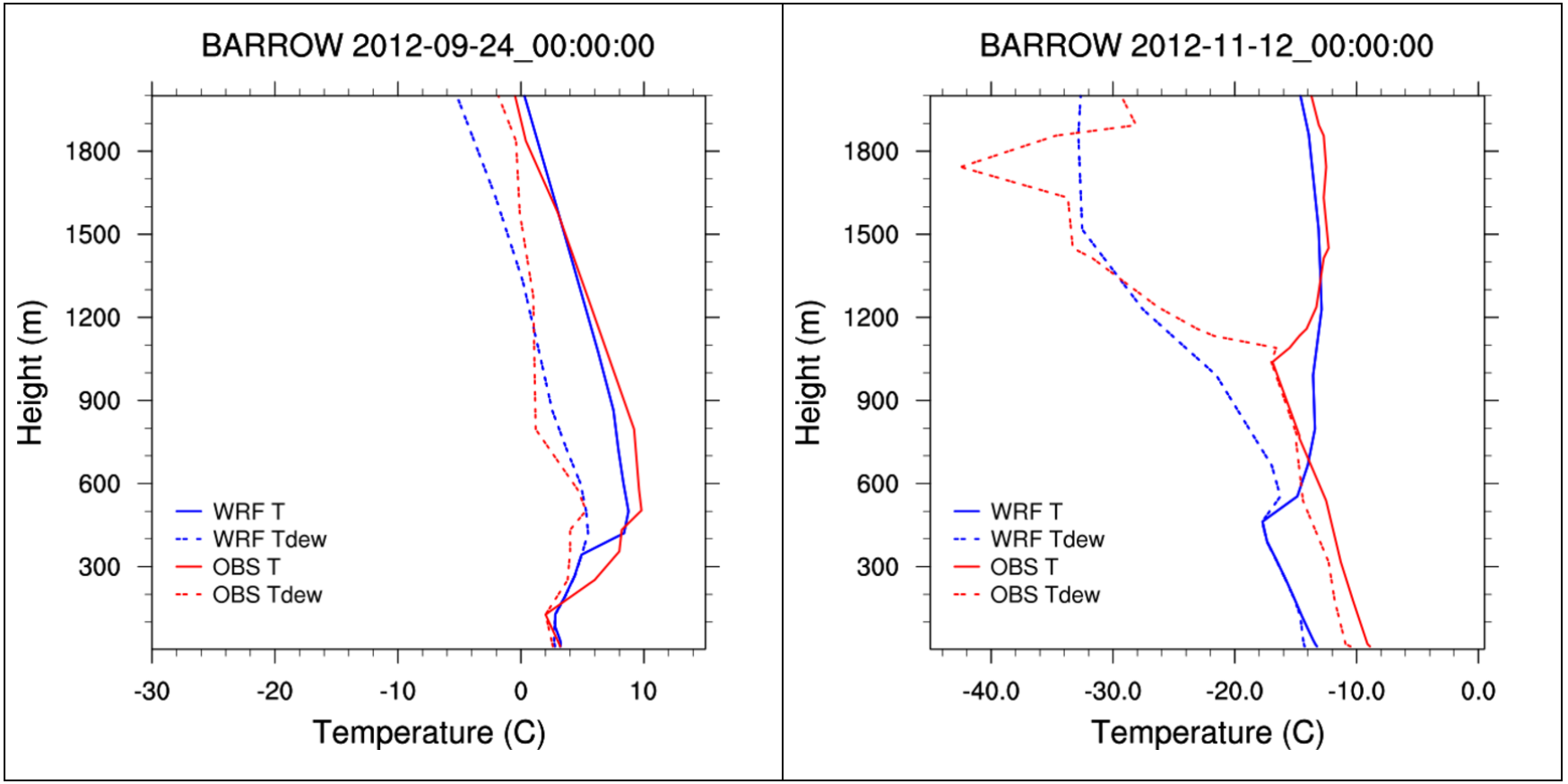

Figure 13. Vertical profile soundings comparing BOEM Arctic WRF to upper-air data at Point Barrow, AK (PABR) on September 24, 2012 and November 12, 2012 at 00 UTC

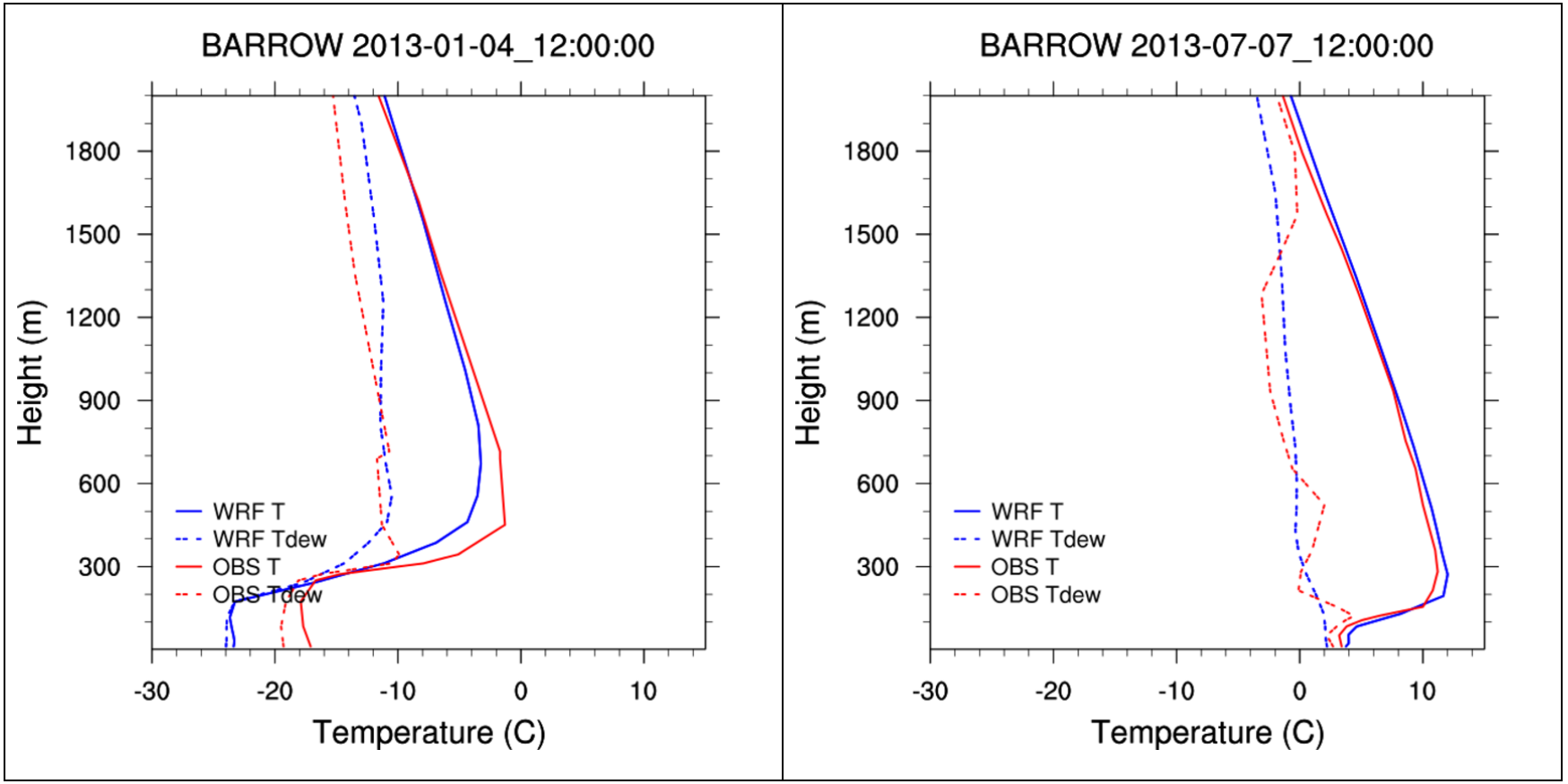

Figure 14. Vertical profile soundings comparing BOEM Arctic WRF to upper-air data at Point Barrow, AK (PABR) on January 4, 2013 at 12 UTC and July 7, 2013 at 12 UTC

4.3 Qualitative Evaluation Using PRISM Precipitation

This section presents a qualitative comparison of WRF simulation estimated monthly precipitation with monthly "normal" PRISM precipitation estimates. Five-year average (2009-2013) monthly precipitation plots were constructed from BOEM Arctic WRF output and compared to PRISM 30-year average monthly plots.

The Parameter-elevation Regressions on Independent Slopes Model (PRISM) datasets are spatial maps of climate elements across the United States built by the Spatial Climate Analysis Service at Oregon State University (SCAS-OSU). Gridded maps of mean monthly and annual precipitation and temperature were built using meteorological station measurements and a set of statistical weighting procedures and corrections based on distance, elevation, topographic orientations and influences, and land-surface type (SCAS-OSU, 2001). The process and results have been extensively peer-reviewed and generally accepted by the climatological community as state-of-the-art representations.

The high-resolution Alaska PRISM dataset contains 30-year average (1971-2000) monthly precipitation and temperature over the entire onshore areas of Alaska at 400 m resolution. The dataset was built using measurements from over 732 surface stations and 1637 upper-air grid points from the North American Regional Reanalysis. The data point locations are set in NAD83 Albers projection.

Ramboll Environ obtained the dataset from The Climate Source, Inc., which is the commercial distribution company formed to distribute SCAS-OSU products, and stored it on its servers for the statistical evaluation.

To facilitate the comparison of PRISM to WRF, the PRISM monthly precipitation datasets were transformed from their original NAD83 Albers projection to the given BOEM Arctic WRF projection for all three domains. Given the different time spans between the PRISM and WRF monthly precipitation averages, comparisons of the PRISM plots to the following BOEM Arctic WRF plots should be limited to concepts like "is the WRF precipitation consistent with the "normal" precipitation for that month?" It is also noteworthy that the PRISM dataset only covers mainland Alaska, while the BOEM Arctic WRF dataset encompasses the entire domain.

Figure 15 through Figure 19 display spatially the five-year WRF precipitation datasets and the PRISM data for the months of January through May, respectively, in the 4 km domain d03. It is clear that all of these months tend to be quite dry, and both the WRF and PRISM average precipitation plots reflect this. Given the two sets of plots, it is evident that WRF tended to simulate "pockets" of higher precipitation totals than anywhere in the corresponding PRISM datasets. However, WRF also appeared to slightly under-predict winter-spring precipitation totals on a larger scale throughout much of the Brooks Mountain Range which forms the southern border of the North Slope. However, both of these discrepancies could be due in large part to the difference in timescale. The PRISM data was averaged over a much longer span of time, which could have the effect of smoothing out the instances of higher precipitation, while accounting for some outlier years that include some rainfall in the typically dry areas.

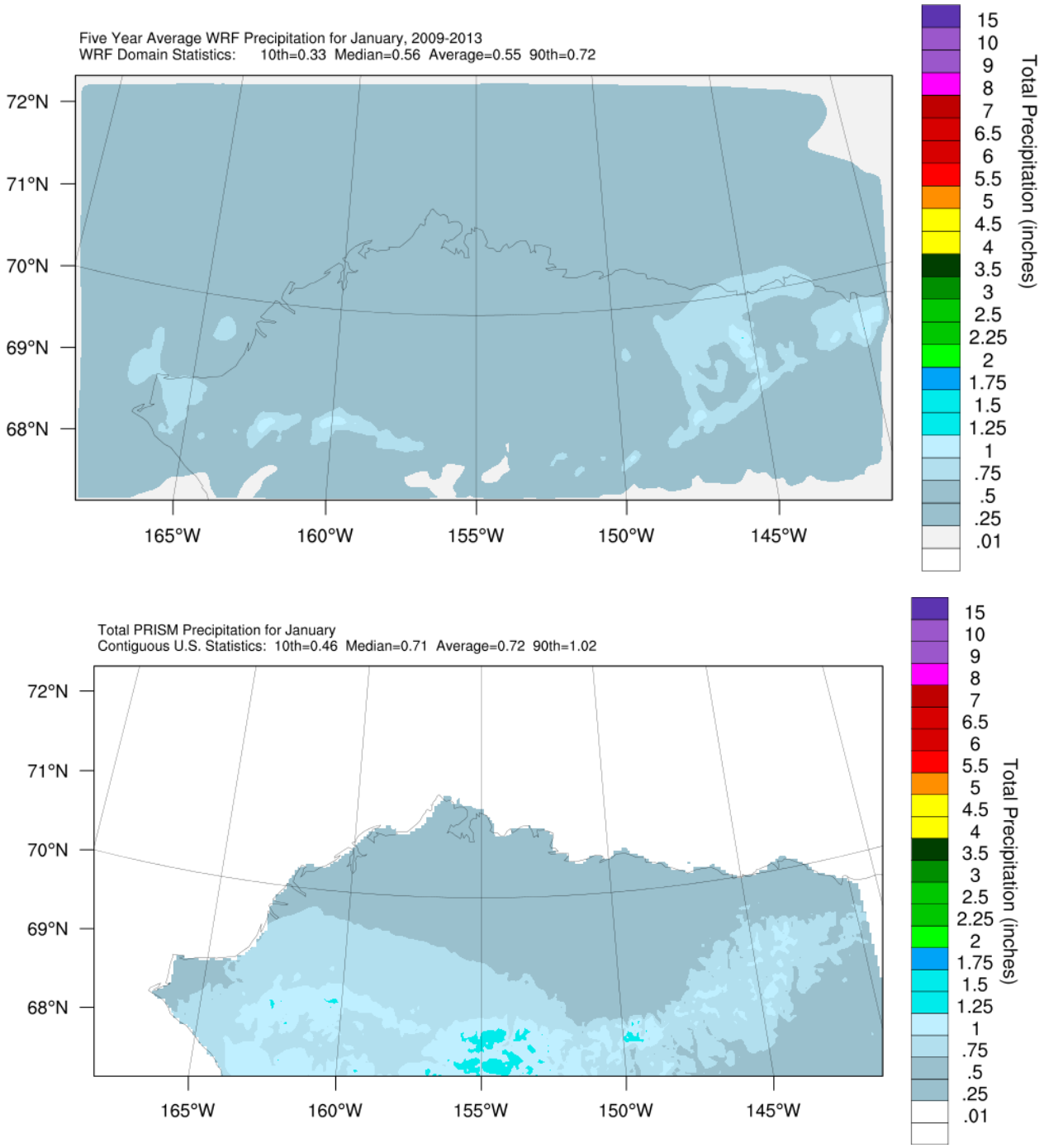

Figure 15. 5-year (2009-2013) WRF precipitation average (top) and 30-year PRISM precipitation average (bottom) monthly precipitation totals for January in the 4 km domain

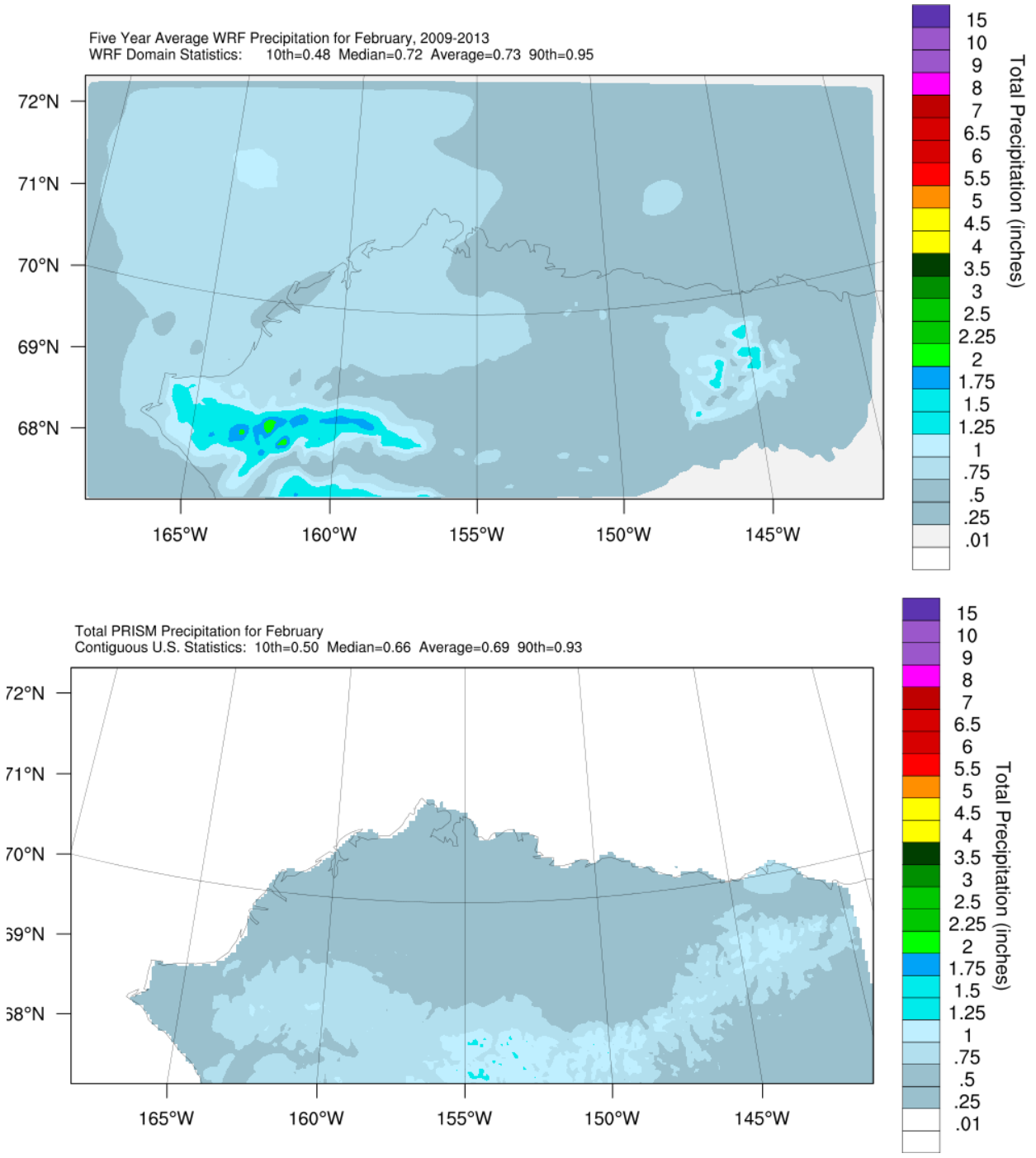

Figure 16. 5-year (2009-2013) WRF precipitation average (top) and 30-year PRISM precipitation average (bottom) monthly precipitation totals for February in the 4 km domain

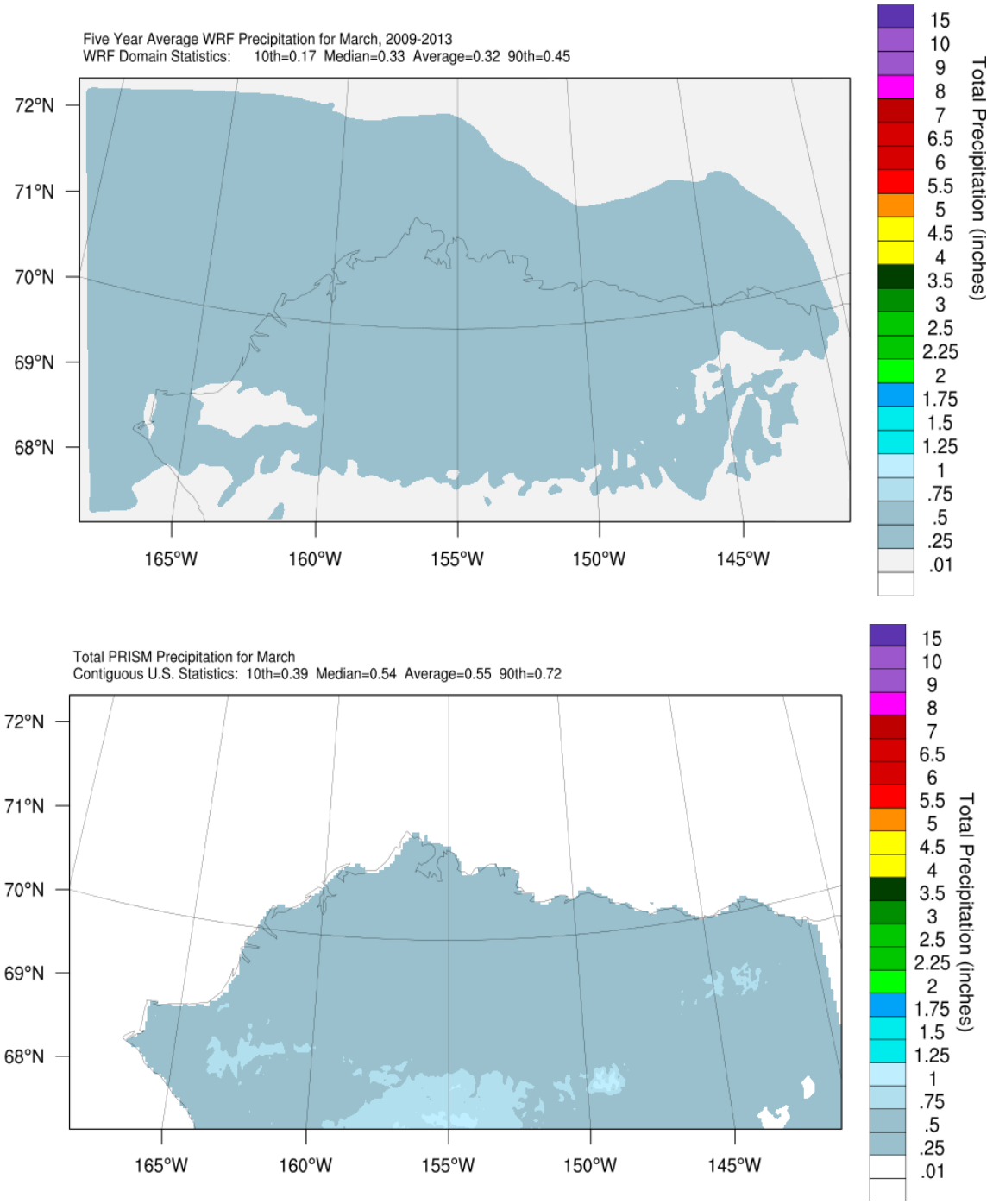

Figure 17. 5-year (2009-2013) WRF precipitation average (top) and 30-year PRISM precipitation average (bottom) monthly precipitation totals for March in the 4km domain

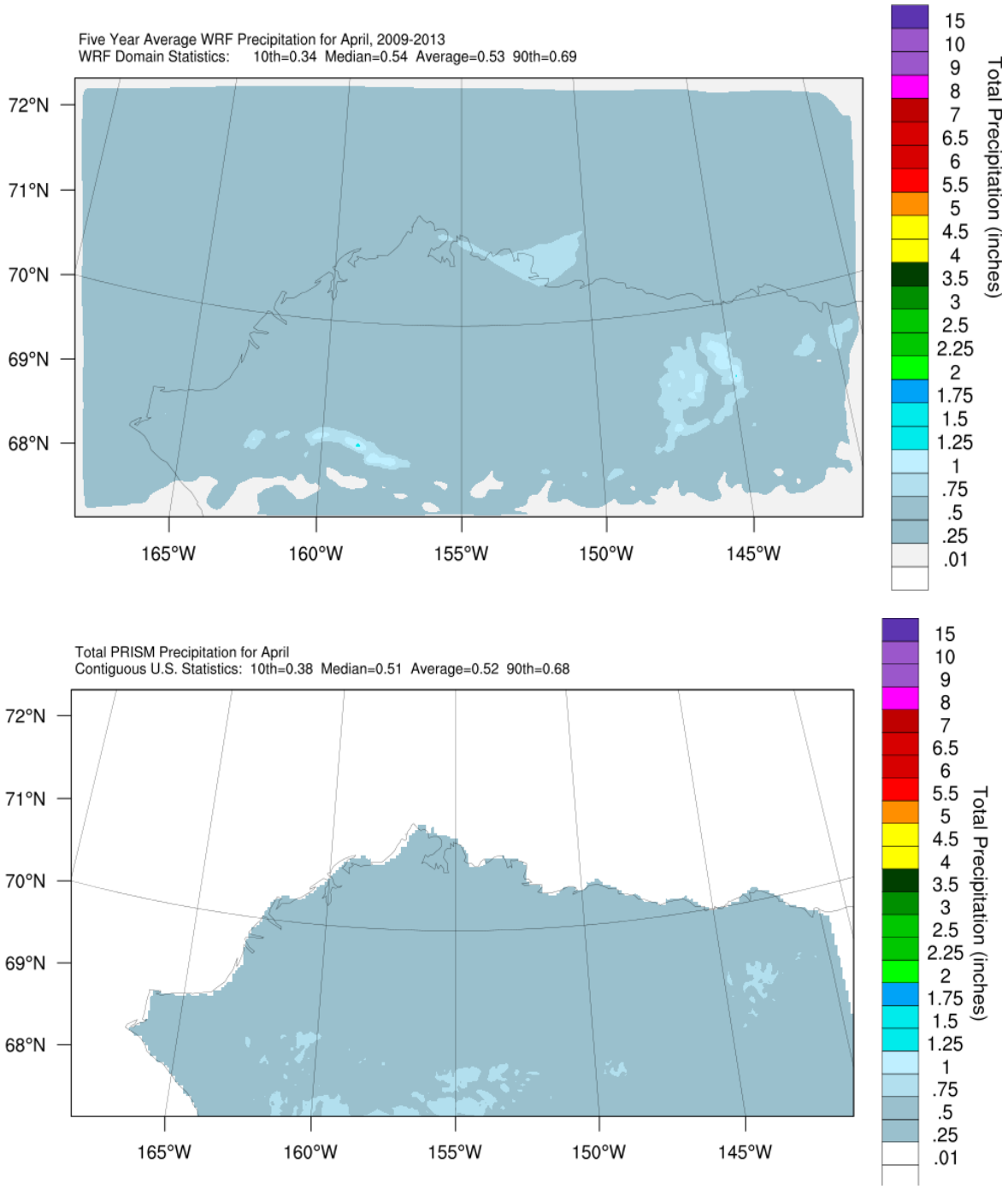

Figure 18. 5-year (2009-2013) WRF precipitation average (top) and 30-year PRISM precipitation average (bottom) monthly precipitation totals for April in the 4km domain

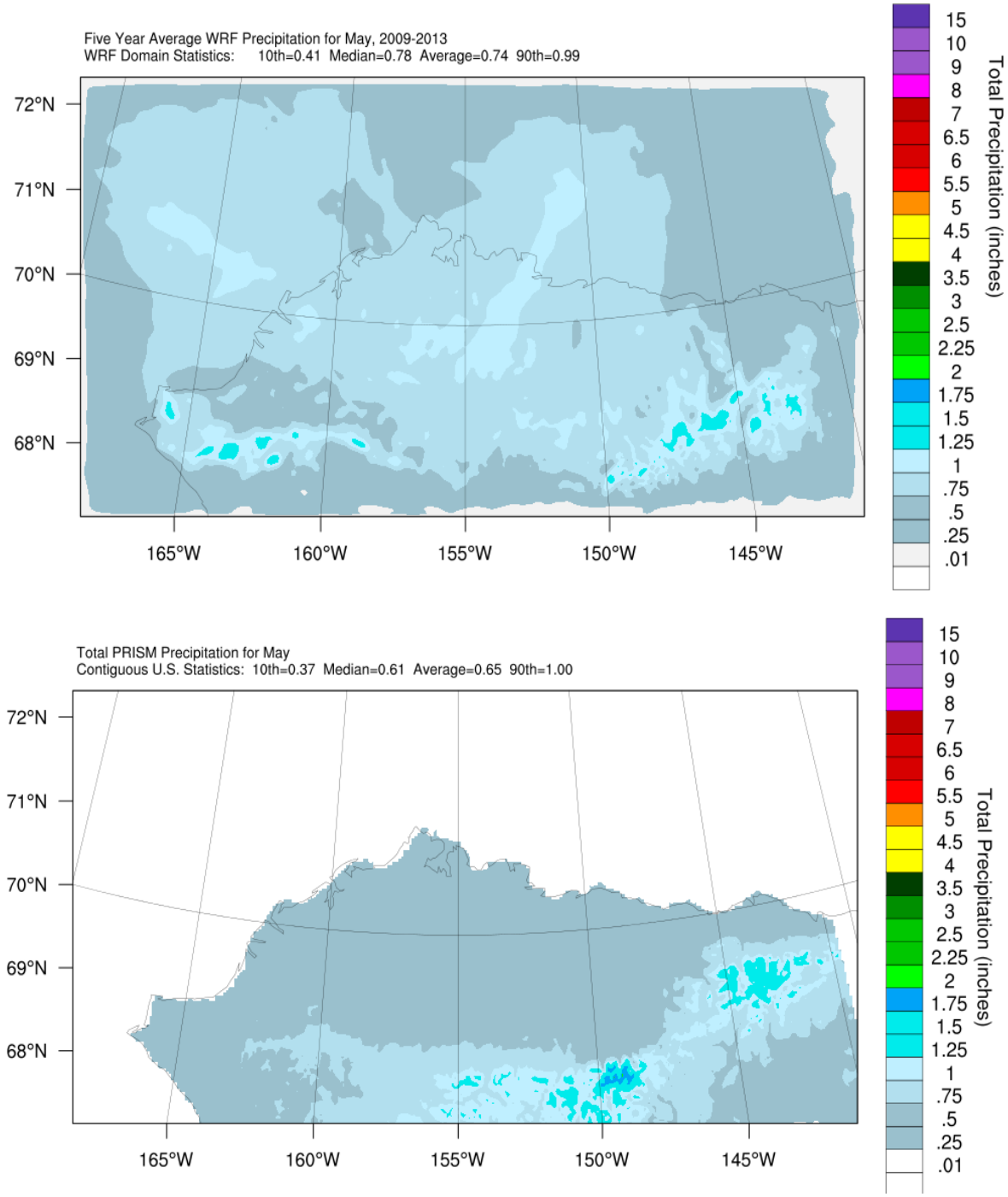

Figure 19. 5-year (2009-2013) WRF precipitation average (top) and 30-year PRISM precipitation average (bottom) monthly precipitation totals for May in the 4km domain

Figures 20 through 22 represent the 4km domain average monthly precipitation plots for WRF forecasts and PRISM observations for June through August, respectively. It is apparent that these summer months are the rainiest in northern Alaska, but also that the majority of the rain is limited to the Brooks Mountain Range on the southern edge of the North Slope. For these three months, the WRF five-year average precipitation plots appear very similar to the PRISM 30-year data. One difference is that the WRF simulations tend to slightly under-predict precipitation in the areas with the highest rainfall.

Figures 23 through 26 show WRF and PRISM average monthly precipitation plots for September through December, respectively, in the 4km domain. The fall months show substantial discrepency between WRF forecast five-year and PRISM observation 30-year average monthly precipitation plots. Particularly in September and October, WRF drastically under-predicts precipitation along the Brooks Mountain Range, while appearing to over-allocate precipitation along the north coast of Alaska. In November and December, observed precipitation totals begin to decrease toward the low winter levels, and these model discepencies become less pronounced. WRF performed well overall, simulating precipitation over onshore portions of the 4 km domain, but tended to under-forecast enhanced rainfall areas over more complex conditons in and around the Brooks Mountain Range.

4.4 Qualitative Evaluation Using Satellite Cloud Cover Observations

The dataset selected for this study is the MISR Level 3 Monthly FIRSTLOOK Component cloud product derived from the Multi-angle Imaging Spectro-Radiometer (MISR) instrument measurements. The MISR is an instrument deployed aboard the NASA Terra satellite. The product selected is the derivation of monthly averaged spatial cloud cover fraction on a 0.5° by 0.5° horizontal resolution. Cloud cover fraction is computed for a set of vertical levels at 500 m resolution. The dataset from 2005-2013 was obtained from the online NASA Atmospheric Science Data Center, located at (https://eosweb.larc.nasa.gov/project/misr/level3/overview).

MISR retrievals of cloud cover fraction (CCF) were compared qualitatively to estimates calculated from WRF. WRF calculates fractional cloud cover at each level of each grid point (output as variable “CLDFRA”). The maximum cloud fraction over the vertical column was identified at each grid point and assumed to represent the total cloud cover fraction (cloud cover fraction of an area as seen from the surface). This method introduces error because varying degrees of cloudiness at different heights could result in a total cloud cover fraction (cloud cover fraction as seen from the ground) that is greater than, but not less than, the fraction at any given level. Therefore, this approach could be expected to produce a negative bias in total cloud cover fraction.

The mean monthly CCF at each grid point was calculated, resulting in 12 plots per year for each domain of the 2009-2013 WRF simulations. The monthly MISR satellite CCF is calculated for 45 vertical levels at 500 m resolution. The maximum CCF over the vertical column was identified at each grid point and assumed to represent the total CCF, as was done to estimate WRF cloud fractions. Again, it is expected that such estimates would have a negative bias because they do not account for the additive effect of cloud cover at different levels. However, since the purpose of the comparison is to evaluate WRF performance and both datasets may result in negative bias, the bias is likely inconsequential unless one dataset introduces substantially more bias than the other.

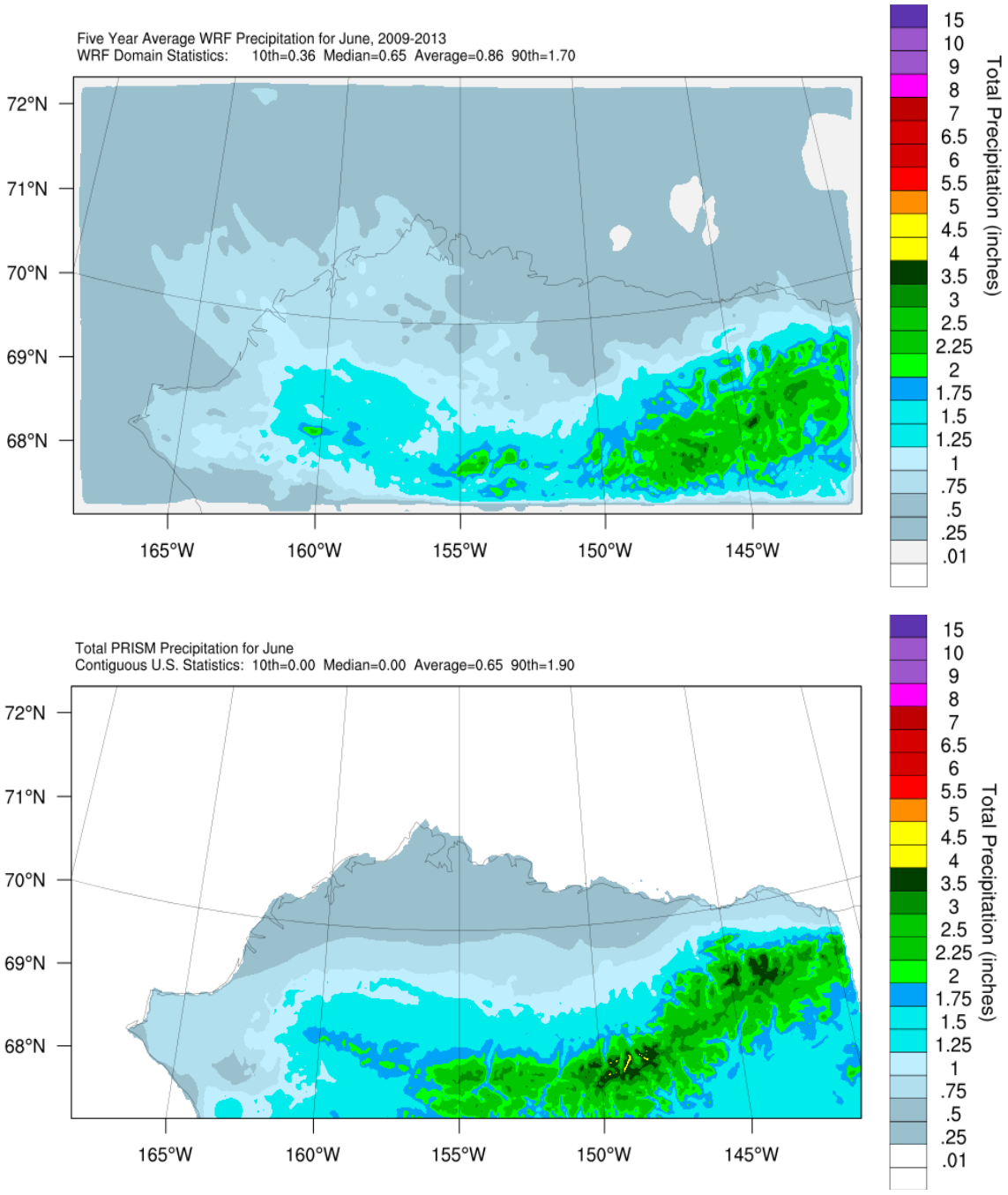

Figure 20. 5-year (2009-2013) WRF precipitation average (top) and 30-year PRISM precipitation average (bottom) monthly precipitation totals for June in the 4km domain

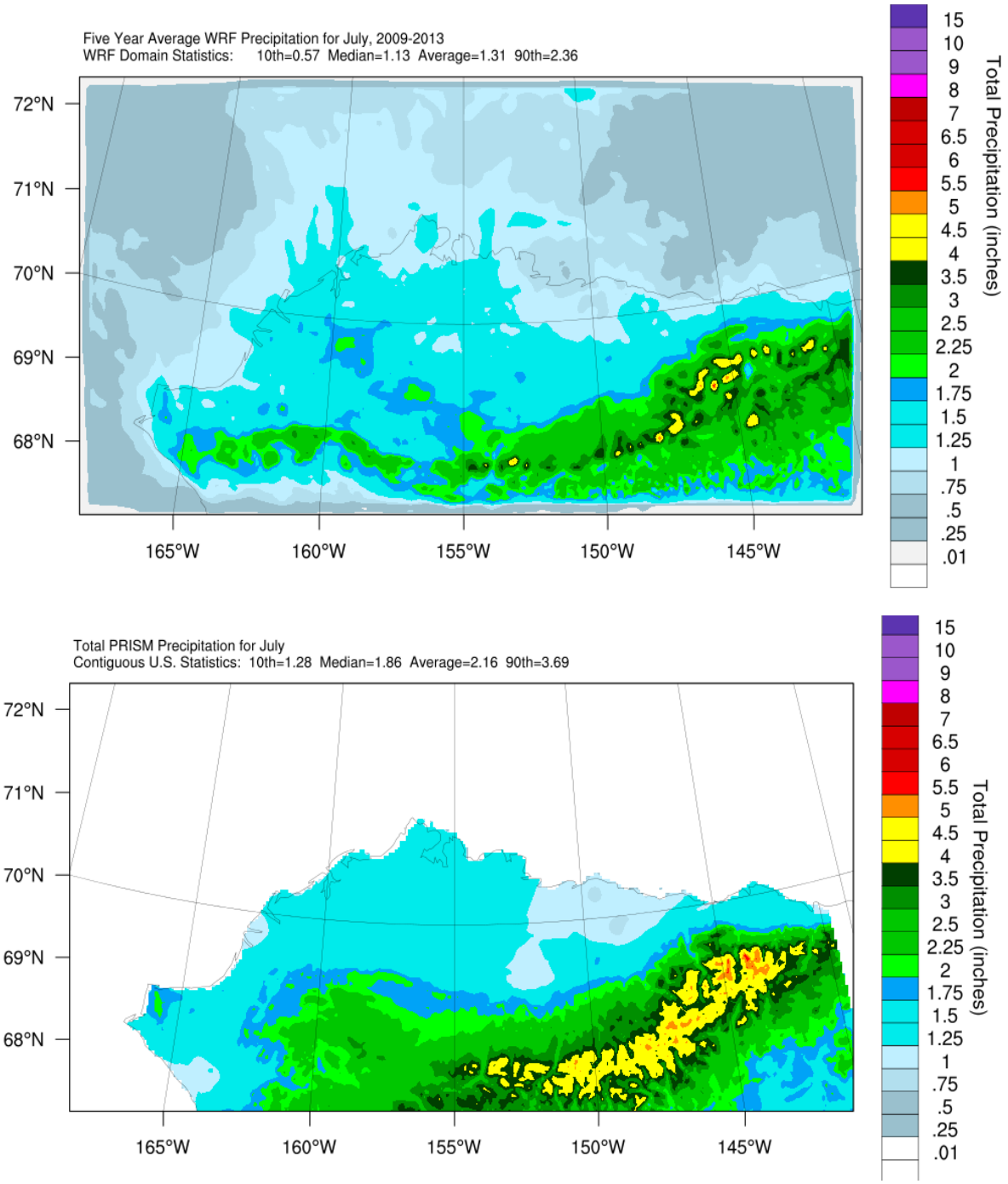

Figure 21. 5-year (2009-2013) WRF precipitation average (top) and 30-year PRISM precipitation average (bottom) monthly precipitation totals for July in the 4km domain

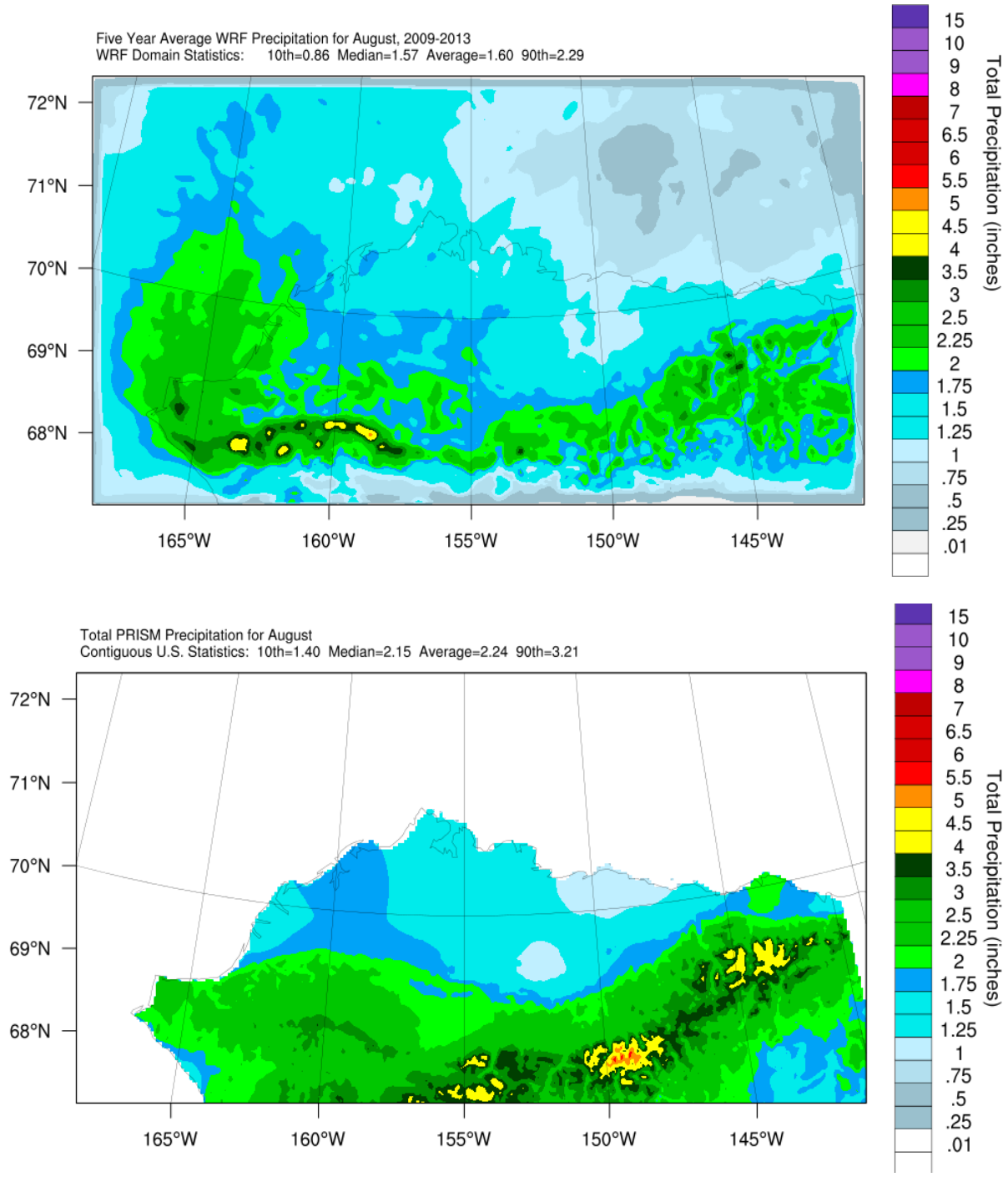

Figure 22. 5-year (2009-2013) WRF precipitation average (top) and 30-year PRISM precipitation average (bottom) monthly precipitation totals for August in the 4km domain

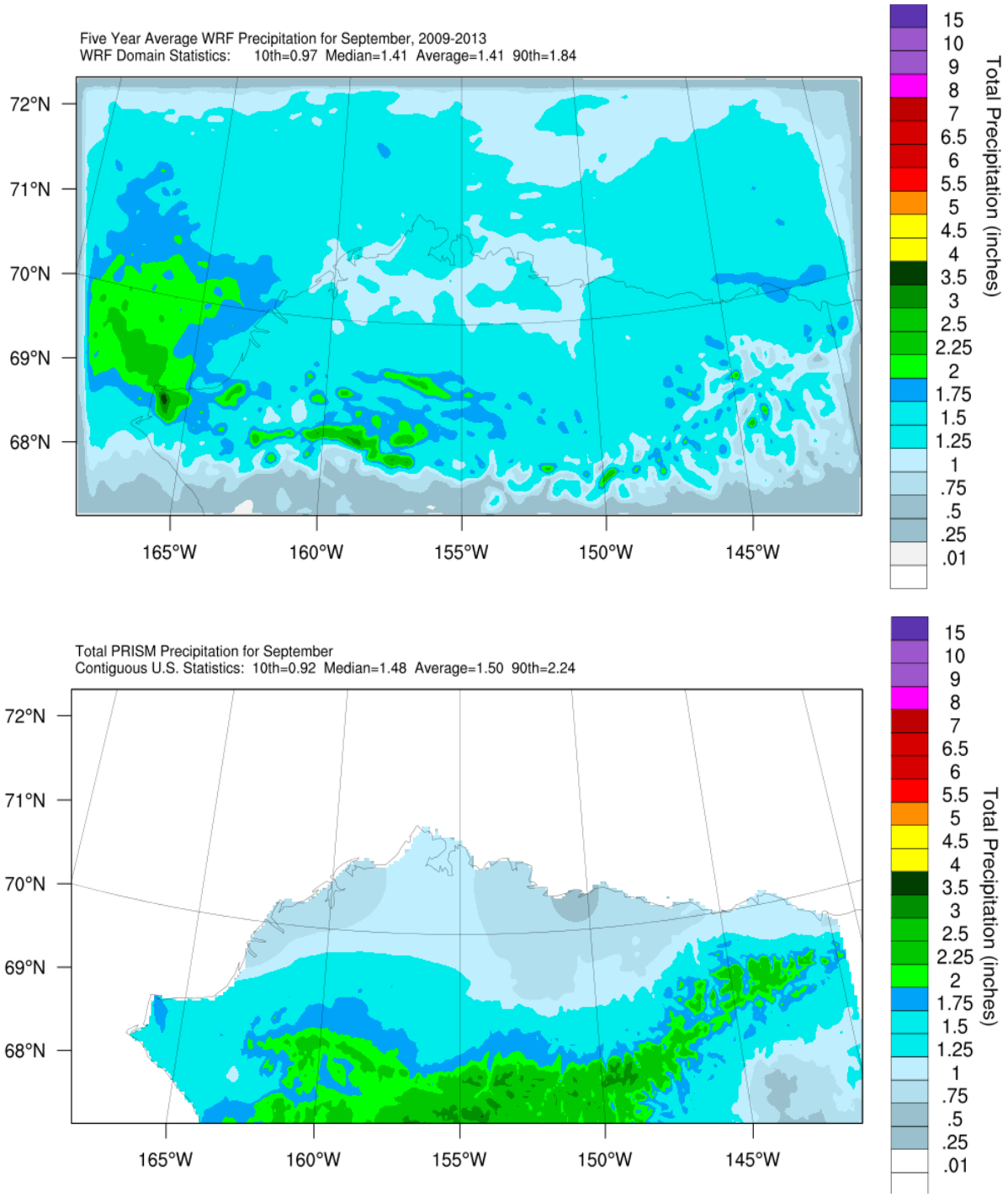

Figure 23. 5-year (2009-2013) WRF precipitation average (top) and 30-year PRISM precipitation average (bottom) monthly precipitation totals for September in the 4km domain

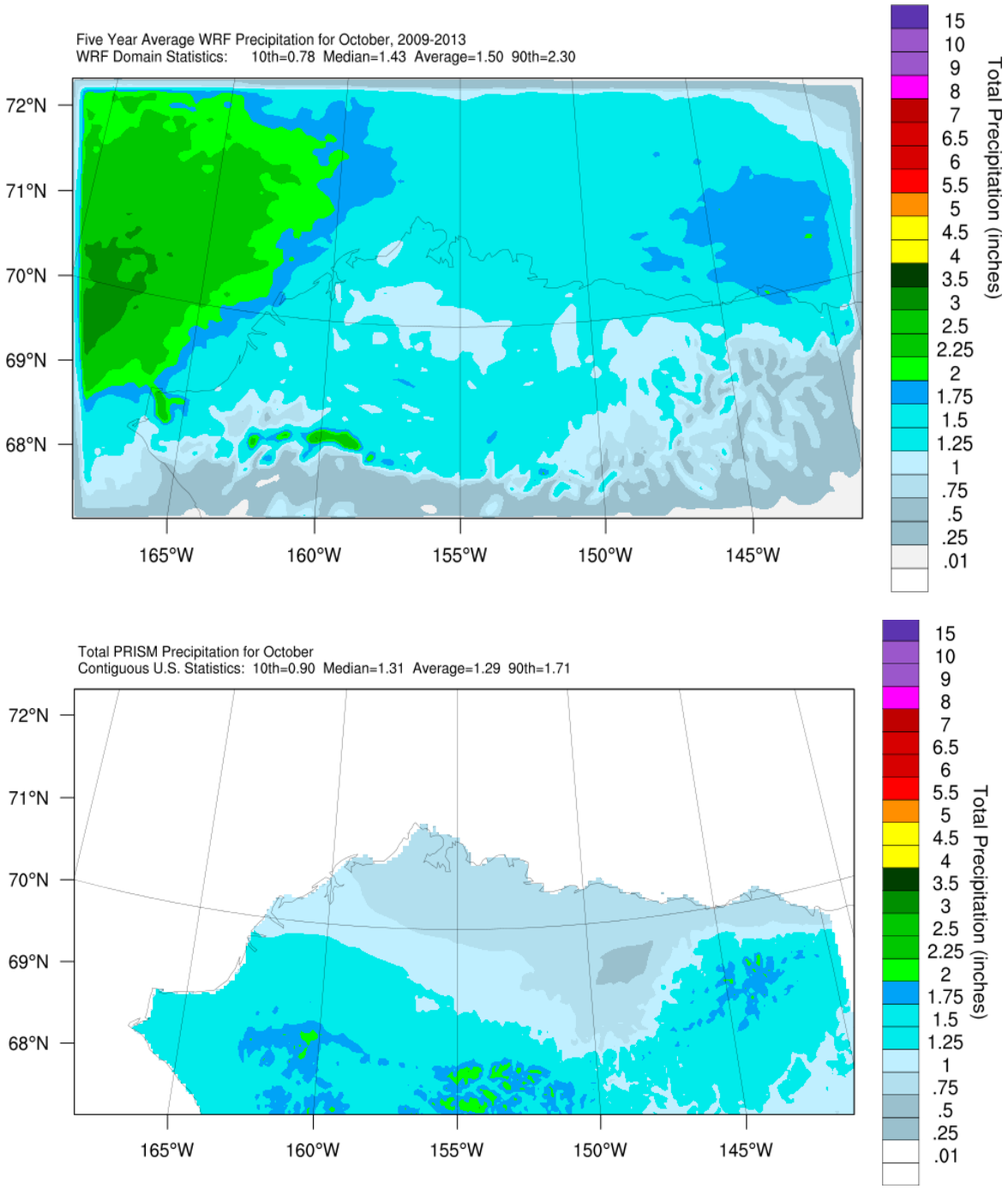

Figure 24. 5-year (2009-2013) WRF precipitation average (top) and 30-year PRISM precipitation average (bottom) monthly precipitation totals for October in the 4km domain

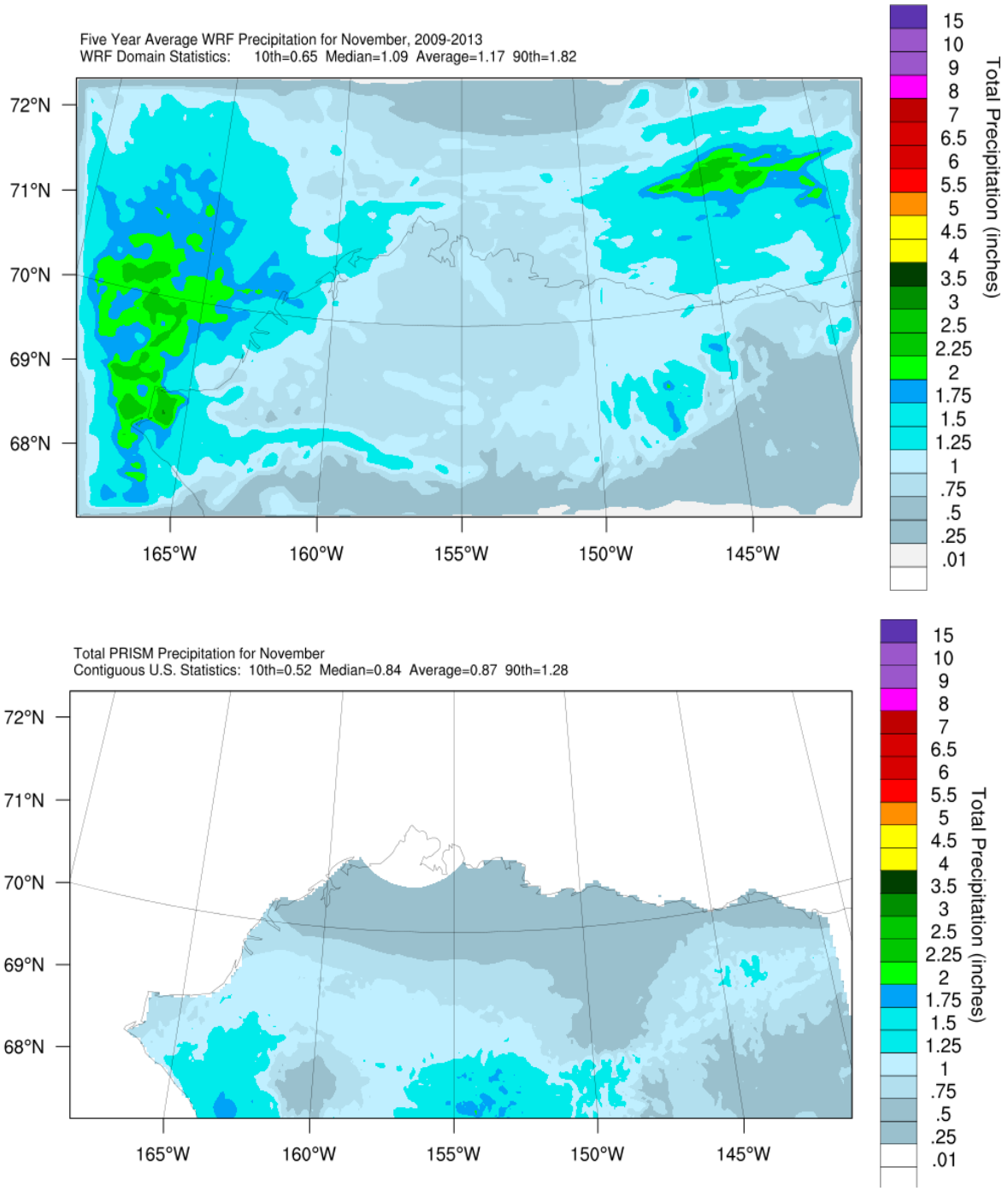

Figure 25. 5-year (2009-2013) WRF precipitation average (top) and 30-year PRISM precipitation average (bottom) monthly precipitation totals for November in the 4km domain

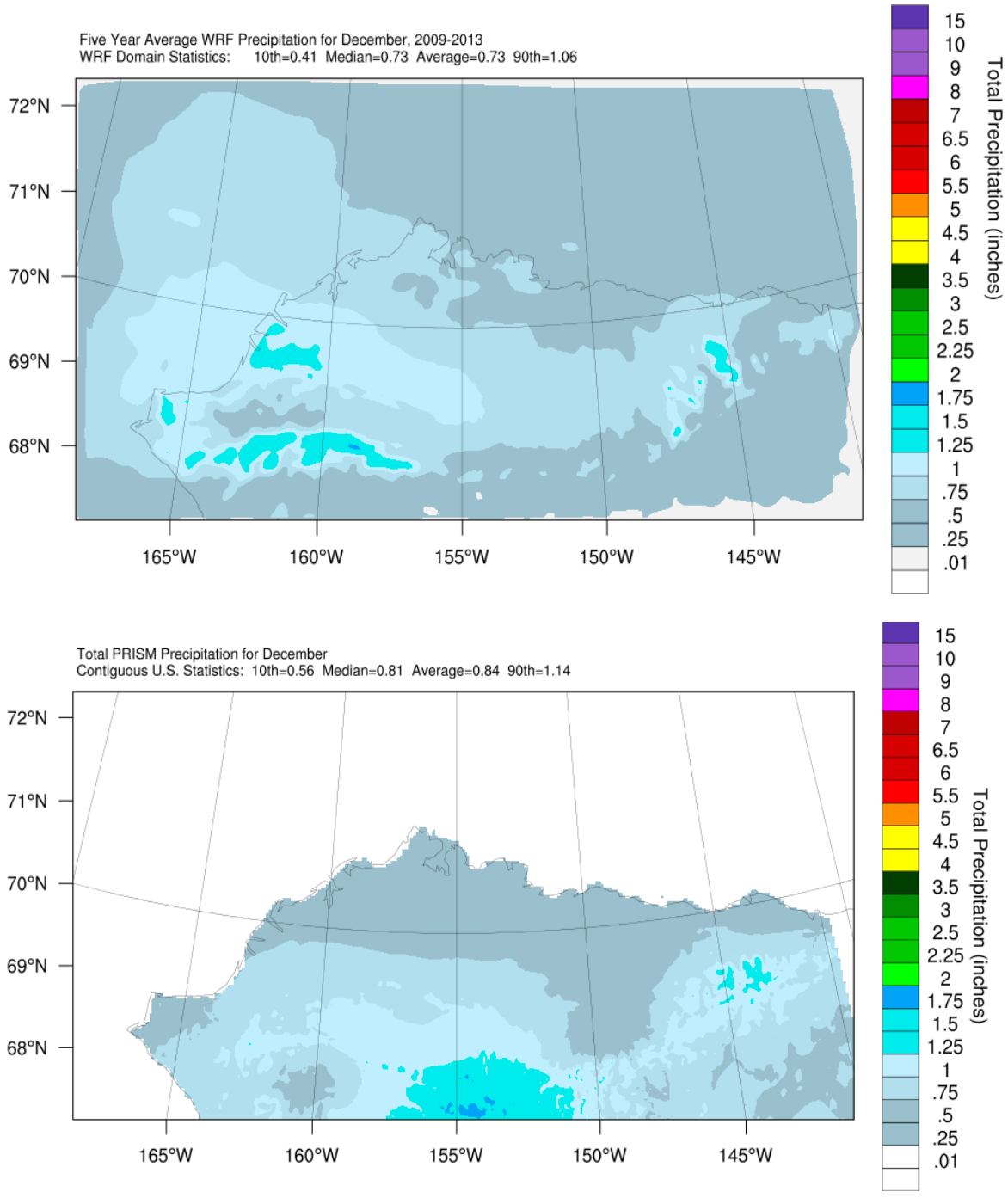

Figure 26. 5-year (2009-2013) WRF precipitation average (top) and 30-year PRISM precipitation average (bottom) monthly precipitation totals for December in the 4km domain

The monthly MISR CCF was re-projected to match the projection and horizontal resolution of the WRF domains. Plots of monthly MISR CCF were produced for the 36km (domain 1), 12km (domain 2), and 4km (domain 3) domains for direct comparison to BOEM Arctic WRF results.

Also, note that MISR estimates cloud fraction using visible wavelengths. Cloud fraction cannot be accurately estimated for a portion of the domain during winter months due to the lack of sunlight in the Arctic. MISR also uses a snow/ice mask in regions where ice and snow cover the surface. Based on the qualitative examination summarized in this section, it appears that MISR CCF estimates may not be reliable during winter months. The influence of surface ice and snow and lack of sunlight in the Arctic in winter months introduces error, appearing to result in a negative cloud cover bias.

The qualitative comparison of WRF and MISR CCFs was focused on domain 2 of the WRF simulations. Domain 1 WRF resolution is the most similar to the resolution of the MISR dataset, but domain 2 provided a more focused examination of the area of interest.

An annual pattern in the MISR data was evident comparing the five years of data. MISR CCF distribution was noisy and low during the winter months (November – April). It appears that MISR data is likely unreliable as an accurate source of CCF during these months. During these periods when average MISR CCF is relatively low (0.3 -0.4) and noisy, WRF average CCF is relatively high (0.8 – 0.9) and forms distinct patterns including heavy cloud cover over the North Slope and Arctic Ocean. An example of these differences is shown in Figure 27 for January 2011.

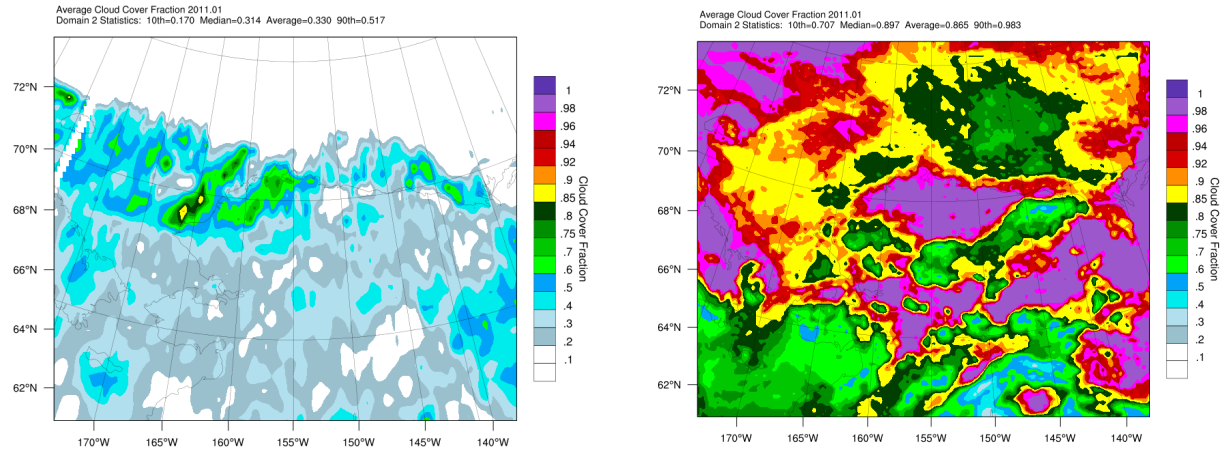

Figure 27. MISR (left) and WRF (right) CCF, January 2011

In March, the MISR data is punctuated by a region of higher CCF along the central inland north slope (with CCF of 0.5-0.6). The regional CCF peak is evident in most March WRF run cases also. An example of this feature is shown in Figure 28 for March of 2011. By March, the WRF

domain is less CCF saturated than the earlier months and distinct patterns are visible. All years except for 2012, inland cloud cover becomes less pervasive, dampening from an average of 0.8 - 0.9 in the earlier months to an average in the range of 0.6 – 0.7. CCF over the Arctic Ocean dampens also, with the saturated CCF values greater than 0.9 covering less area.

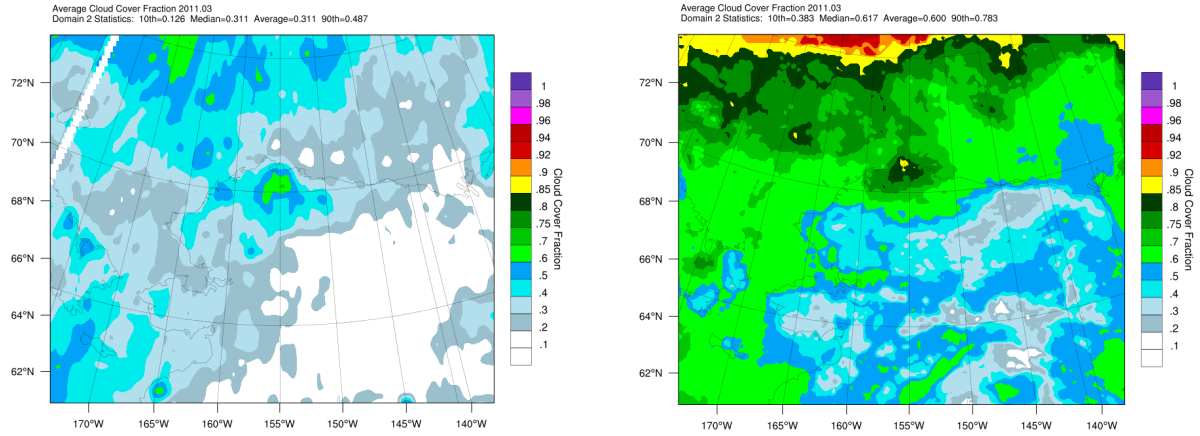

Figure 28. MISR (left) and WRF (right) CCF, March 2011

By April, the patterns of cloud cover distribution in the MISR data become more defined and less noisy. A common feature is the concentration of higher CCF in the range of 0.5 to 0.8 over the Chukchi Sea and along the coast of the Beaufort Sea. This pattern is reflected in the WRF results but with higher magnitude CCF in the range of 0.8 – 0.95. This is best demonstrated in the April 2012 results shown in Figure 29.

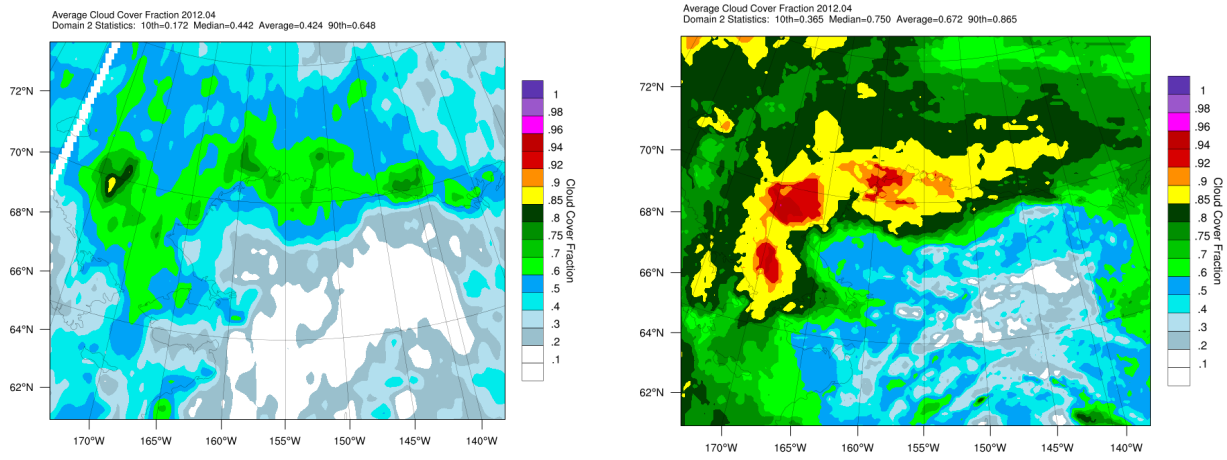

Figure 29. MISR (left) and WRF (right) CCF, April 2012

By May, the MISR data appear to be much less affected by ice/snow/low-light return problems given that the CCF distribution is distinct and less noisy across the domain. All five years of April MISR, except 2009, portray a similar pattern characterized by a mass of higher CCF (in the range of 0.7 – 0.9) in the Chukchi Sea and Arctic Ocean in the northwest corner of the domain. In 2009, the mass of higher CCF concentrates more in the Beaufort Sea and the Arctic Ocean in the northeast corner of the domain. This pattern is also evident in the WRF data, characterized by a concentration of higher CCF values (0.85 – 1.0) over the Chukchi Sea and Arctic waters in the northwest of the domain. The WRF and MISR features most closely match in the May 2011 case shown in Figure 30.

For the June cases, the WRF and MISR CCF patterns appear to not agree as well as the May cases. The MISR cases are punctuated by bands of high CCF (in the range of 0.9 – 1.0) over the Bering Sea all five years. A narrow band of high CCF is also evident along the Beaufort Sea coastline all five years. MISR CCF over the Arctic Ocean is widespread, but lower in magnitude (0.5 – 0.7 on average) than the WRF results (0.8 – 0.9 on average). Higher values of CCF are evident over the inland areas of Alaska in both the MISR and WRF datasets. Bands of higher CCF are evident along the Brooks Range of mountains in both MISR and WRF datasets. The inland and marine CCF features discussed are evident in the June 2009 cases shown in Figure 31.

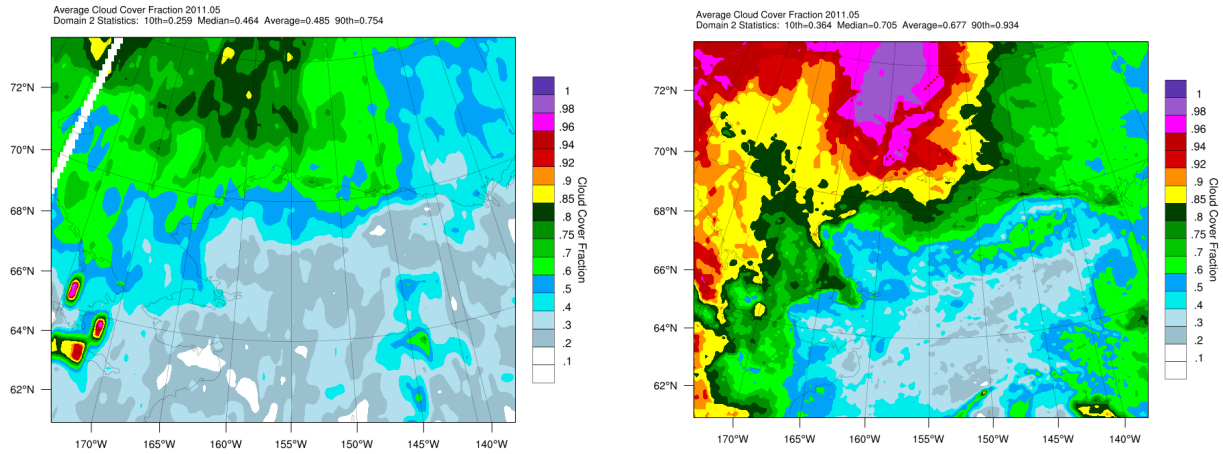

Figure 30. MISR (left) and WRF (right) CCF, May 2011

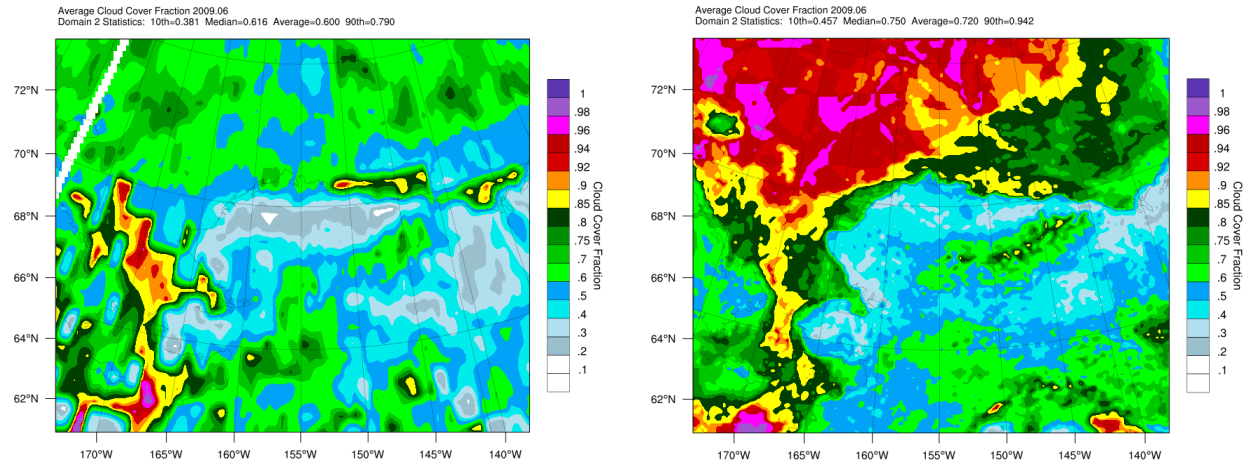

Figure 31. MISR (left) and WRF (right) CCF, June 2009

For July, the MISR cases have a similar pattern as seen in June. The Bering Sea is dominated by high CCF cover in the range of 0.8 to 1.0. The shape and magnitude of the Bering Sea CCF pattern is captured well in the WRF simulations, as seen in Figure 32 for the July 2009 case. However, the WRF CCF over the Arctic Ocean is more widespread and higher in magnitude than the MISR data. It is unlikely that MISR data suffers from lack of visible light in July, but the data may still be biased due to ice and snow cover over the Arctic Ocean. It is unknown to what degree the remaining ice cover has on the MISR data. It is possible that the MISR data have low bias and WRF highly over-predicts CCF. However, given the increase in MISR CCF in August over all five years, we assume that the July MISR data is biased low over the Arctic.

In August there is a markedly large increase in MISR CCF over the Beaufort and Chukchi Seas. MISR continues to measure widespread high CCF values over the Bering Sea and Strait as well. WRF under-predicts CCF in the Bering Sea/Strait compared to MISR with average values in the range of 0.8 – 0.9 compared to MISR values in the 0.9 – 1.0 range. WRF agrees well with patterns and magnitudes of CCF in the MISR dataset over the Chukchi and Beaufort Seas. However, WRF predicts widespread CCF near 1.0 across the Arctic Ocean, while MISR predicts values in the 0.7 - 0.8 range possibly biased low due to partial ice cover. These patterns are all evident in the August 2013 cases, shown in Figure 33.

WRF and MISR CCF distributions are the most comparable in the September cases compared to all other months. This may be due to the fact that MISR negative bias may be minimized since ice cover extent is usually at its minimum in September. For all five years, the extent and magnitude of WRF CCF matches well to the MISR CCF, particularly over the marine areas. WRF tends to predict higher CCF along the north-central portion of the North Slope. September 2009 and 2012 cases are shown in Figure 34 and Figure 35, respectively, to illustrate these features.

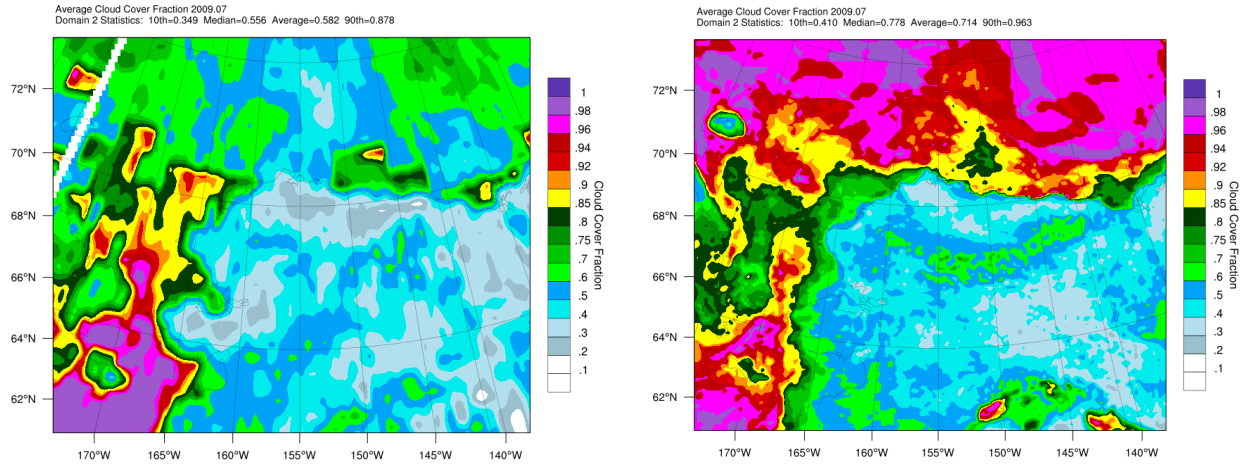

Figure 32. MISR (left) and WRF (right) CCF, July 2009

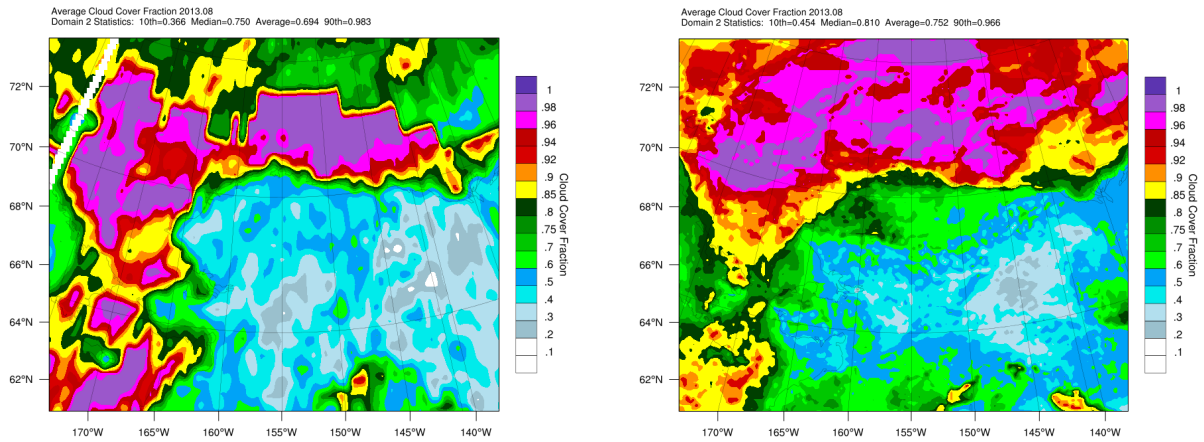

Figure 33. MISR (left) and WRF (right) CCF, August 2013

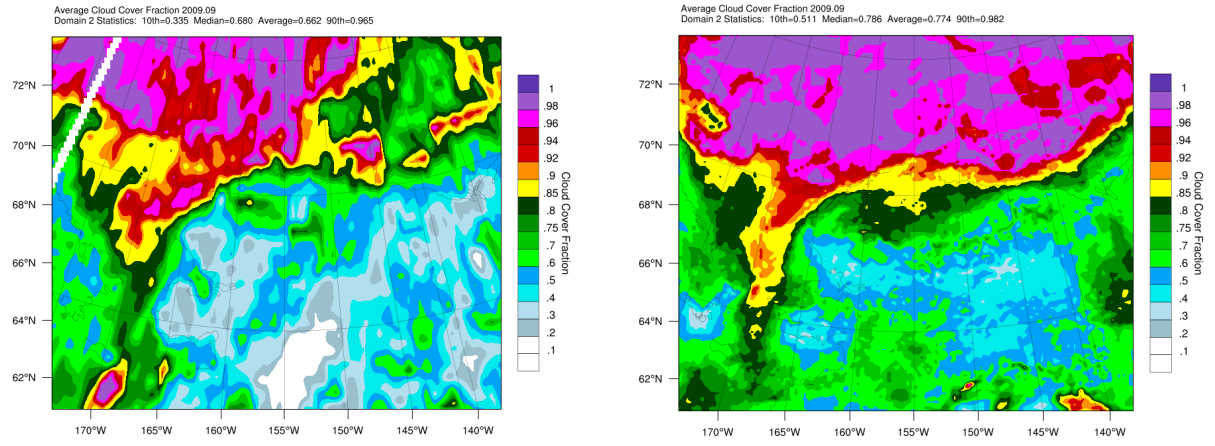

Figure 34. MISR (left) and WRF (right) CCF, September 2009

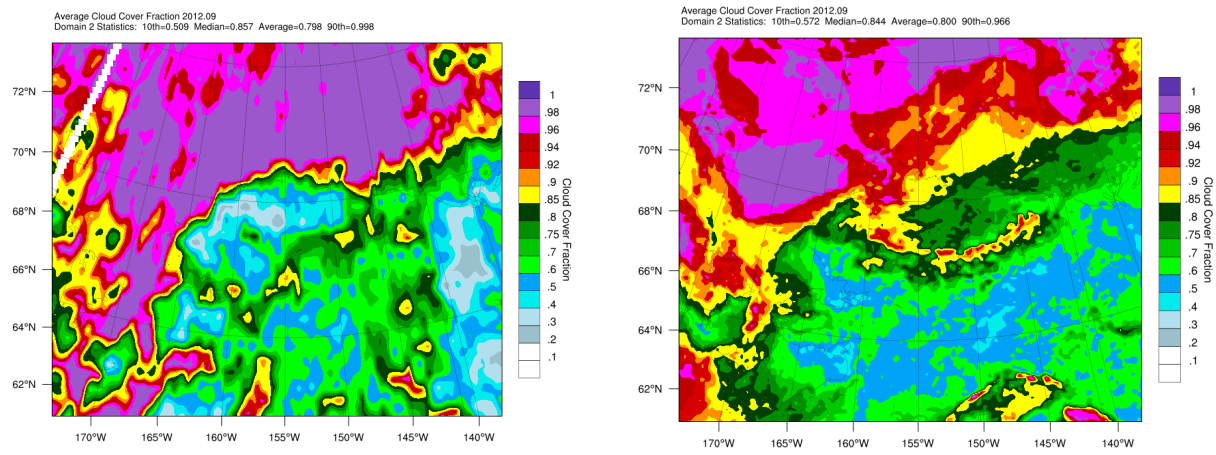

Figure 35. MISR (left) and WRF (right) CCF, September 2012

For the October cases, magnitude and extent of CCF from both MISR and WRF match qualitatively well also. The October MISR data are noisier than the September data and there is evidence that sea ice expanse and limited light may result in bias, particularly over the northern and north-western portions of the domain. Again, WRF tends to be cloudier over land overall. The October 2012 cases are shown in Figure 36 to demonstrate these features.

For November and December it is evident that ice cover and lack of visible light limits the ability of MISR to measure CCF. The MISR data are noisy and average CCF is unnaturally low. WRF CCF coverage is extensive during these winter months. The December 2011 case is shown in Figure 37.

In conclusion, MISR data appear to be unreliable as a source of "true" CCF in the Arctic for a considerable portion of the year due to negative bias resulting from ice-cover interference and insufficient sunlight. MISR data are therefore likely the most reliable in late summer.

Qualitative comparisons of WRF monthly average CCF to MISR CCF in September and October revealed similar spatial distributions and CCF magnitude over much of the domain. WRF CCF over land appeared to be biased high by 5-15% on average.

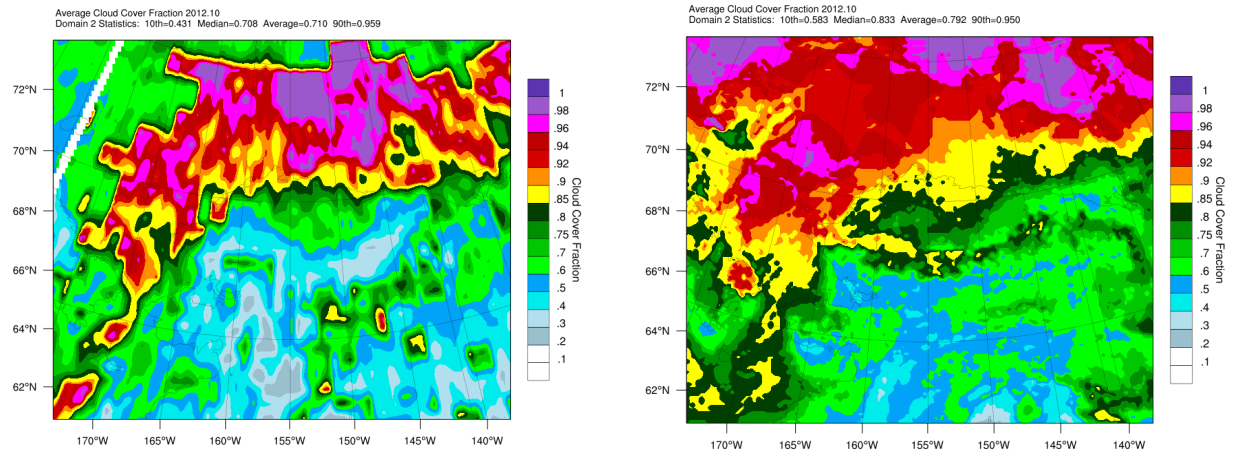

Figure 36. MISR (left) and WRF (right) CCF, October 2012

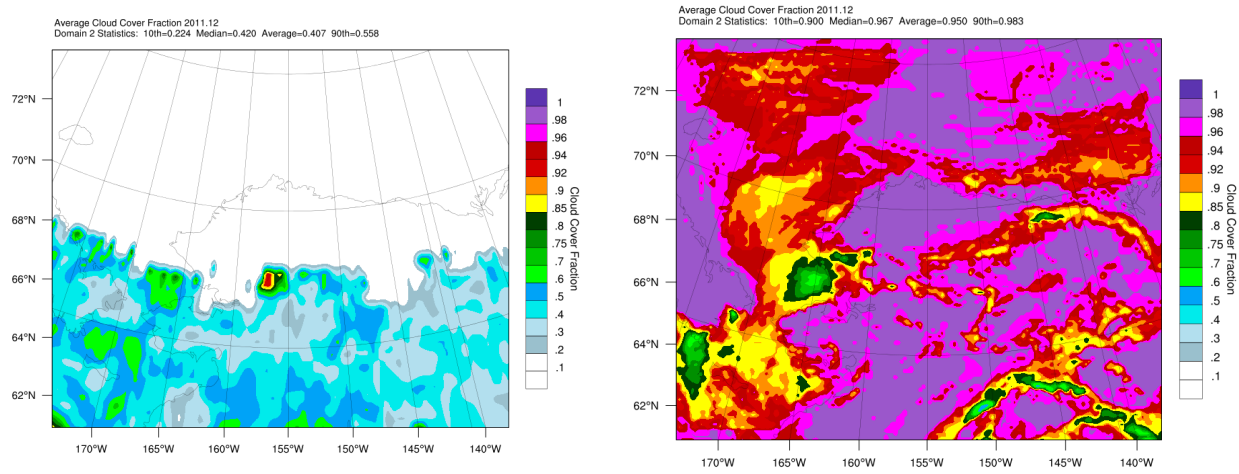

Figure 37. MISR (left) and WRF (right) CCF, December 2011

5.0 SUMMARY AND CONCLUSIONS

The BOEM Arctic January 2009 through December 2013 WRF meteorological model simulation reproduced the observed surface meteorological variables reasonably well. The wind direction performance is improved over previous meteorological datasets for the same region. Vertical profiles also performed well, accurately reproducing observed conditions of coastal interactions in the planetary boundary layer. The 5-year average precipitation amounts for each month were consistent with the PRISM 30-year normal. Where and when valid satellite cloud retrievals were available, WRF-predicted cloud amount compared reasonably well.

Based on our experience, the BOEM Arctic WRF modeling's performance provides a sound basis for developing meteorological inputs for Arctic Air Quality Study modeling.

6.0 REFERENCES

Brashers et al., 2015. *Meteorological Dataset Evaluation – Final Task Report*, BOEM Arctic Air Quality Impact Assessment Modeling Study. By Ramboll Environ, Lynnwood, WA.

Bromwich, D., Hines, K., and Bai, L.-S. (2009). Development and Testing of Polar WRF, Part 2: Arctic Ocean. *J. Geophys. Res.*, D08122.

Chen, F.; Janjic, Z.; Mitchell, K. (1997). Impact of atmospheric surface layer parameterization in the new land-surface scheme of the NCEP Mesoscale Eta numerical model. *Bound.-Layer Meteor.* 391-421.

Emery, C.A., E. Tai, and G. Yarwood. 2001. *Enhanced Meteorological Modeling and Performance Evaluation for Two Texas Ozone Episodes.* Prepared for the Texas Natural Resource Conservation Commission (now TCEQ), by ENVIRON International Corp, Novato, CA. Available at: http://www.tceq.texas.gov/assets/public/implementation/air/am/contracts/reports/mm/EnhancedMetModelingAndPerformanceEvaluation.pdf

Kemball-Cook, S., Y. Jia, C. Emery, and R. Morris, 2005. *Alaska MM5 Modeling for the 2002 Annual Period to Support Visibility Modeling.* Prepared for the Western Regional Air Partnership, by ENVIRON International Corp., Novato, CA. Available at: http://pah.cert.ucr.edu/aqm/308/docs/alaska/Alaska_MM5_DraftReport_Sept05.pdf

Hines, K., and Bromwich, D. (2008). Development and testing of Polar WRF, Part 1: Greenland ice sheet meteorology. *Mon. Wea. Rev.*, 1971-1989.

McNally, D. E., 2009. *12 km MM5 Performance Goals.* Presentation to the Ad-Hoc Meteorology Group. June 25, 2009. Available at: http://www.epa.gov/scram001/adhoc/mcnally2009.pdf

NCAR, 2015. National Center for Atmospheric Research. Mesoscale & Microscale Meteorological Laboratory. https://www.mmm.ucar.edu/

NOAA (2015). National Weather Service. National Centers for Environmental Prediction.

http://www.ncep.noaa.gov/

NOAA-NCDC. (2014). NOAA NCDC Integrated Surface Database. Retrieved from **www.ncdc.noaa.gov/isd**
NOAA-NCDC. (2015). Brief Review of Problems and Issues with Integrated Surface Data (ISD). Retrieved from http://www1.ncdc.noaa.gov/pub/data/inventories/ish-qc.pdf

NOAA-OFCM. (1997) Federal Meteorological Handbook No. 3 Rawinsonde and Pibal Observations. Office of the Federal Coordinator for Meteorology. Available at http://www.ofcm.gov/fmh3/pdf/04-chap4.pdf

NOAA-NODC. (2014). NOAA NODC Ocean Archive System. Retrieved from www.nodc.noaa.gov/cgi-bin/OAS/prd/accession/93399

SCAS-OSU, 2001. Climate Mapping with PRISM. Oregon State University (OSU)